The Impact of El Niño–Southern Oscillation (ENSO) on Winter and Early Spring U.S. Tornado Outbreaks

ASHTON ROBINSON COOK

NOAA/NWS/Storm Prediction Center, and School of Meteorology, University of Oklahoma, Norman, Oklahoma

LANCE M. LESLIE AND DAVID B. PARSONS

School of Meteorology, University of Oklahoma, Norman, Oklahoma

JOSEPH T. SCHAEFER

Embry–Riddle Aeronautical University, Daytona Beach, Florida

(Manuscript received 15 July 2016, in final form 27 March 2017)

ABSTRACT

In recent years, the potential of seasonal outlooks for tornadoes has attracted the attention of researchers. Previous studies on this topic have focused mainly on the influence of global circulation patterns [e.g., El Niño–Southern Oscillation (ENSO), North Atlantic Oscillation, or Pacific decadal oscillation] on spring tornadoes. However, these studies have yielded conflicting results of the roles of these climate drivers on tornado intensity and frequency. The present study seeks to establish linkages between ENSO and tornado outbreaks over the United States during winter and early spring. These linkages are established in two ways: 1) statistically, by relating raw counts of tornadoes in outbreaks (defined as six or more tornadoes in a 24-h period in the United States east of the Rocky Mountains), and their destructive potential, to sea surface temperature anomalies observed in the Niño-3.4 region, and 2) qualitatively, by relating ENSO to shifts in synoptic-scale atmospheric phenomena that contribute to tornado outbreaks. The latter approach is critical for interpreting the statistical relationships, thereby avoiding the deficiencies in a few of the previous studies that did not provide physical explanations relating ENSO to shifts in tornado activity. The results suggest that shifts in tornado occurrence are clearly related to ENSO. In particular, La Niña conditions consistently foster more frequent and intense tornado activity in comparison with El Niño, particularly at higher latitudes. Furthermore, it is found that tornado activity changes are tied not only to the location and intensity of the subtropical jet during individual outbreaks but also to the positions of surface cyclones, low-level jet streams, and instability axes.

1. Introduction

Public, media, and scientific interest in seasonal forecasts of the frequency and severity of severe weather has grown substantially in recent years, particularly in response to the destruction and human impacts resulting from tornadoes during 2011 (Barrett and Gensini 2013; Allen et al. 2015). In that year, numerous significant tornado outbreaks occurred across large areas east of the Rocky Mountains, resulting in over 500 deaths, thousands of injuries, and more than $10 billion in damage (NOAA/NCDC 2011; NOAA 2014). The 2011 season had the second-highest number of tornadoes on record extending back to the 1950s (NOAA 2014), with numbers of fatalities not seen since the 1970s, before the widespread use of Doppler radar to issue advanced short-term warnings. The sequence of tornado outbreaks that occurred during 25–28 April 2011 alone produced over 300 tornadoes confirmed by the National Weather Service (NWS). The 2011 severe weather season had such a detrimental societal impact that the U.S. presidential administration mentioned the need for seasonal forecasts of tornadic activity, similar to the hurricane seasonal outlook produced by NOAA's Climate Prediction Center (CPC) and other groups (Thompson 2016). Following the format of the hurricane seasonal outlooks, such guidance would not be intended to predict the precise timing and location of individual tornadic storms or outbreaks. Instead, the aim would be

Corresponding author: Ashton Robinson Cook, ashton.robinson@noaa.gov

DOI: 10.1175/JAMC-D-16-0249.1

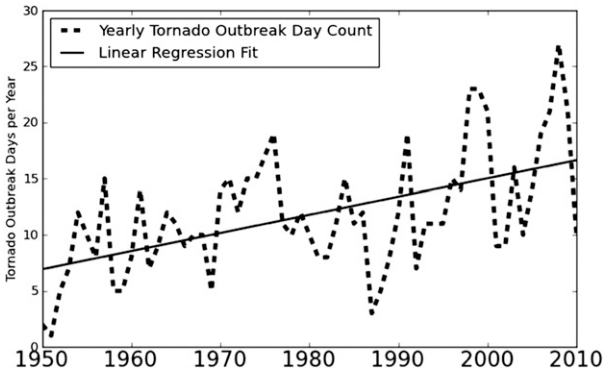

FIG. 1. Yearly counts of January–April tornado outbreak days from 1950 to 2010 for the entire study region ($r^2 = 0.28$).

to provide guidance on the level of severe weather occurrences expected in the upcoming months, including, for example, whether tornadic activity will be below, near, or above normal in various regions of the country.

One promising approach to seasonal forecasting of tornadic activity is to link variations in the frequency of tornadic storms to slowly varying conditions over the Pacific, such as the phase and magnitude of El Niño (EN)–Southern Oscillation (ENSO). Knowles and Pielke (2005) found statistically significant increases in strong tornadoes and "large number outbreaks" during the cool phase of ENSO [La Niña (LN)]. Marzban and Schaefer (2001) struggled to find statistically significant relationships between U.S. tornado activity and ENSO but did mention that the strongest relationship identified in their study was located between sea surface temperatures in the central Pacific and the northeastern United States (from Illinois to the Atlantic coast and from Kentucky to Canada). Cook and Schaefer (2008) showed that winters with neutral (N) ENSO patterns in the tropical Pacific sea surface temperatures had a tendency for tornado outbreaks to be stronger and more frequent than during a warm phase of ENSO (El Niño). During La Niña winter periods, the frequency and strength of U.S. tornado activity lies between that of the neutral and El Niño phases. Cook and Schaefer (2008) also found statistically significant shifts related to

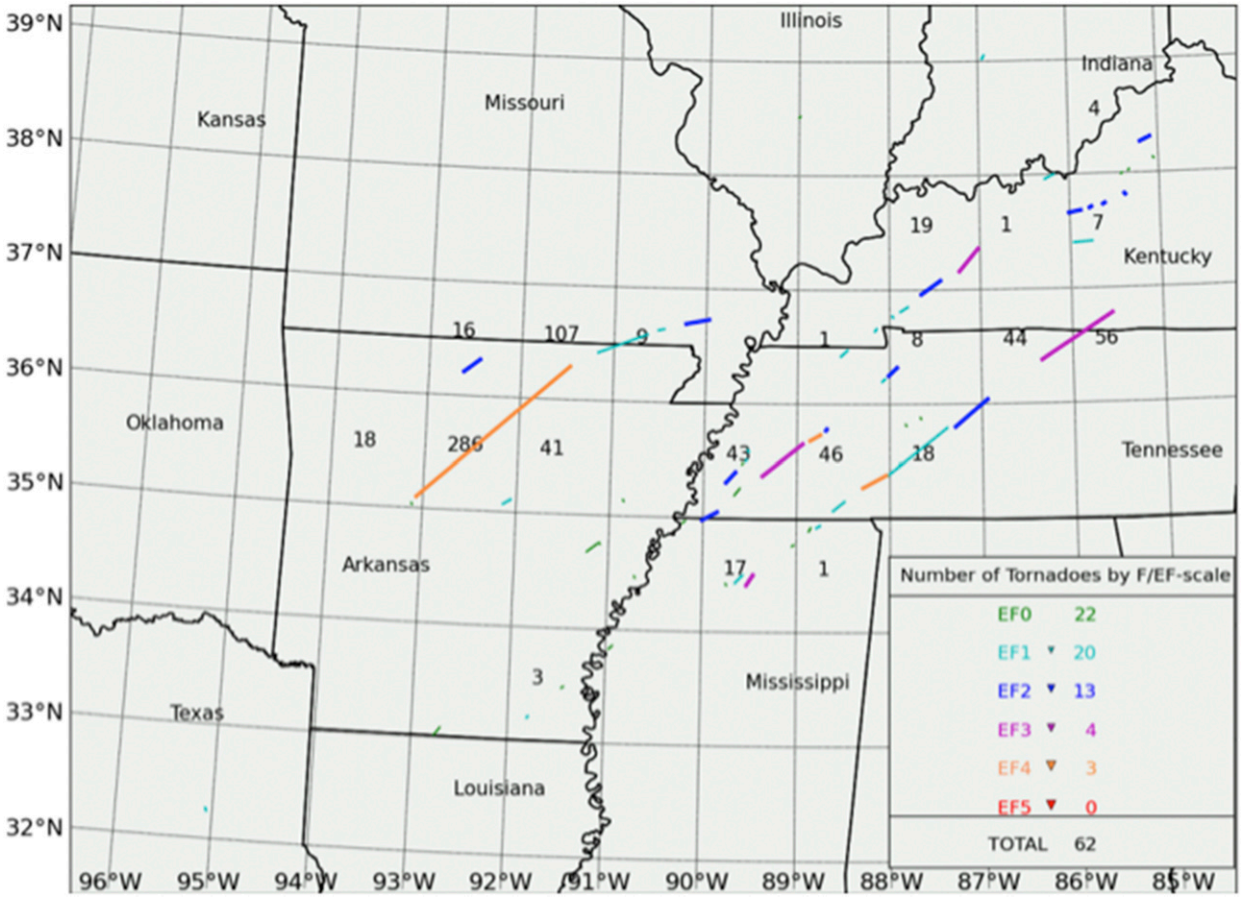

FIG. 2. Example of 1° latitude by 1° longitude gridded DPI calculations using tornadoes from the Super Tuesday tornado outbreak of 5 Feb 2008.

TABLE 1. Synoptic-scale atmospheric features of interest and variables used to identify them. PCAs are conducted on the atmospheric variables for multiple subsets of outbreaks to determine the presence and character of the four ingredients and their associated synoptic-scale atmospheric features. Wind fields are derived from results of PCAs of geopotential height (as described in subsequent paragraphs).

Synoptic-scale atmospheric features of interest	Atmospheric variable used to identify features	Contribution toward tornado outbreaks
Upper-tropospheric jet stream	300-hPa geopotential height, *U* and *V* wind	Lifting mechanism, shear
Surface cyclones	Sea level pressure, *U* and *V* wind	Lifting mechanism, shear
Lower-tropospheric jet stream (LLJ)	850-hPa geopotential height, *U* and *V* wind	Lifting mechanism, shear
Static instability	Lifted index	Instability
Moisture	Precipitable water	Moisture

ENSO patterns in the preferred locations of tornadic activity. These variations of tornadic activity with ENSO phases are also physically plausible. For example, ENSO modulates the mean latitudinal position of the subtropical jet stream across North America (Lee and Galway 1956; Miller 1972; Rasmusson and Mo 1993; Cook and Schaefer 2008; NOAA/CPC 2015; Allen et al. 2015; Lee et al. 2016), which is a key factor for the development of tornado outbreaks (Schaefer 1986; Johns and Doswell 1992).

Linkages between tornadic outbreaks and ENSO may be used to indicate high or low tornadic activity for weeks, and even months, in advance given the persistence and slowly varying nature of ENSO (Cook and Schaefer 2008). More recent studies have focused on other sea surface temperature patterns and global circulation patterns that impact variations in tornado outbreaks over the United States during spring (April and May). For example, Muñoz and Enfield (2011) found an enhancement of the intra-Americas low-level jet stream during La Niña, which was associated with an increased influx of moisture and an increased occurrence of tornadoes to the east of the Mississippi River. Lee et al. (2013) further investigated the ENSO linkages to tornado frequency, finding that despite weak correlations between the Trans-Niño Index and tornado outbreaks, the decay or development of ENSO (Trans-Niño) could produce a pattern of warm sea surface temperatures in the eastern tropical Pacific and cool temperatures in the central Pacific that were more conducive for the development of spring tornado outbreaks. Tippett et al. (2015) presents a comprehensive review of ENSO and additional large-scale influences on severe weather variability, including the Madden–Julian oscillation (MJO) (Madden and Julian 1972). Elsner and Widen (2014) also present linkages between Great Plains tornadoes and sea surface temperatures (SSTs) in the Gulf of Alaska and the western Caribbean Sea.

A major goal of this study is to further explore winter and early spring tornado forecast potential by diagnosing the influence of El Niño/La Niña on January–April 1950–2010 U.S. tornado outbreaks. Allen et al. (2015) had a similar goal, and their study identified general increases in the frequency of severe weather events (both tornadoes and hail) that occurred during La Niña conditions in the equatorial Pacific. That study additionally found that La Niña conditions also were associated with a northward expansion in the latitude of tornadic events as a physical response to the seasonal mean position of the jet stream and instability axes as shown in Allen et al. (2015), with decreases and southward displacement of activity during El Niño. The current study is intended to explore further the linkages between ENSO and tornadic events while also extending the recent results of Allen et al. (2015) and other previous work:

1) It will assess how synoptic-scale atmospheric features that are commonly associated with individual tornado outbreaks shift with ENSO. Such an approach allows linkages to be established between individual outbreaks and ENSO by investigating variability within individual outbreaks and outbreak subsets. This type of climatological assessment of atmospheric factors (i.e., jet streams, surface cyclones, geopotential height troughs, etc.) in outbreaks also offers important insights regarding catalysts for upward vertical motion and convective development that instability- and/or shear-based environmental tornado indices cannot offer [Tippett et al. (2012) used convective precipitation

TABLE 2. Number of times each month was classified as an EN, LN, or N ENSO phase for the period January–April 1950–2010. Months were classified on the basis of the Niño-3.4 SST anomaly. Months containing a Niño-3.4 SST anomaly ≥ 0.5 were classified as El Niño. Months with a Niño-3.4 SST anomaly ≤ -0.5 were classified as La Niña. All other months were classified as N.

	January	February	March	April
EN	21	13	10	12
LN	21	18	17	16
N	19	30	34	33

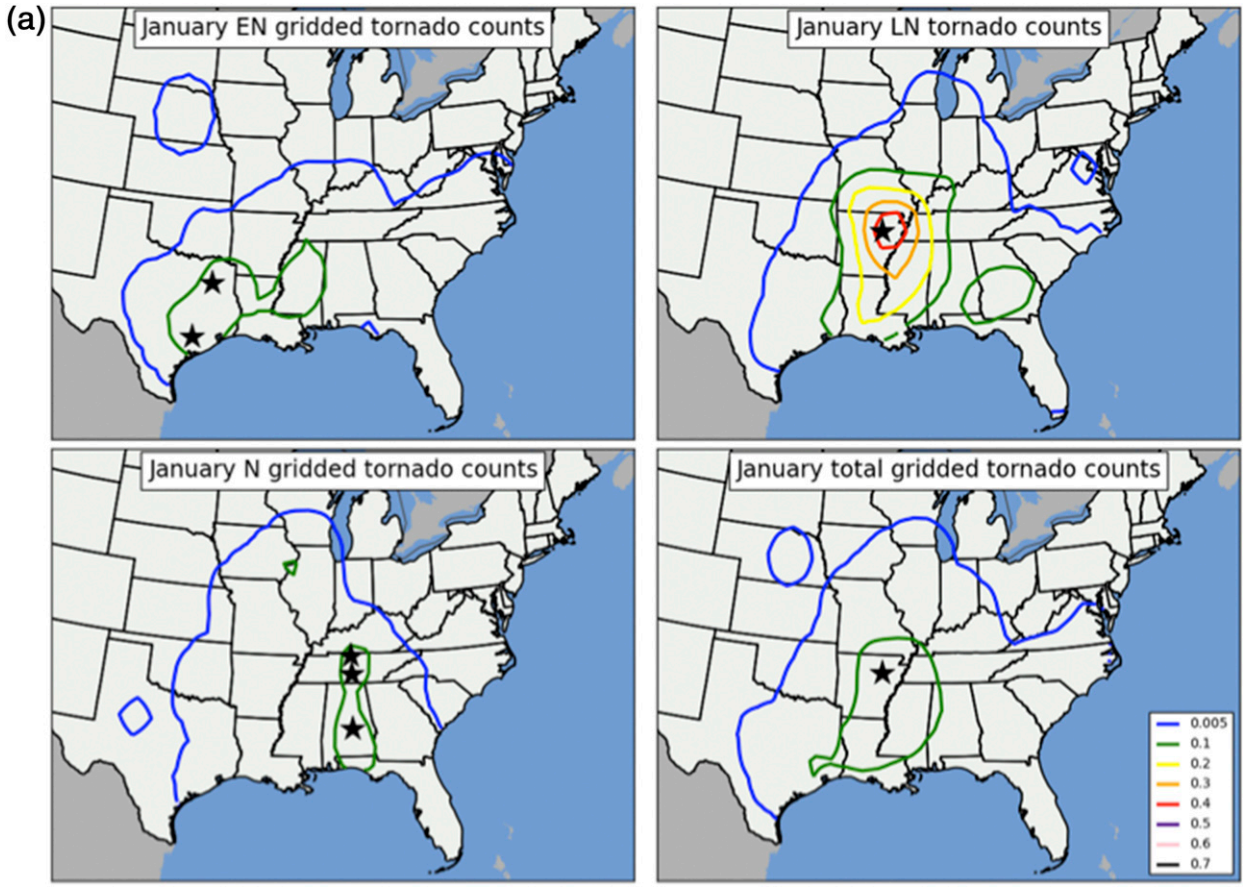

FIG. 3. Contour plots representing normalized gridded tornado counts during (a) January, (b) February, (c) March, and (d) April in each ENSO phase. Tornado data were normalized against the respective number of Januaries, Februaries, Marches, and Aprils classified as El Niño, La Niña, and neutral (Table 2). The black stars indicate locations of maximum normalized tornado occurrences.

in reanalyses as a proxy for lift in their index, although it is heavily dependent on the reanalyses' convective parameterization scheme]. Although environments containing favorable shear and instability for tornadoes occur regularly (especially in spring across the U.S. Great Plains), these environments often do not yield tornadoes unless an impetus for upward vertical motion is present.

2) It will relate various phases of ENSO to variations in tornado counts, tornado days, and the destruction potential index (DPI). Although reporting biases and errors associated with historical tornado records are well documented (Doswell and Burgess 1988; Verbout et al. 2006; Brooks et al. 2003), gridded analyses of these metrics can offer insights regarding location and frequency of higher-impact tornado events within outbreaks, especially when combined with unbiased atmospheric analyses. This approach does not suffer from a failure to distinguish between actual tornado events and the occasional false alarms that occur with the use of environmental severe weather indices.
3) It will include tornado outbreaks dating back to 1950 so as to provide a basis for a more robust atmospheric climatology in this study when compared with that of Allen et al. (2015) (who employed data only back to 1979) and other previous studies (Muñoz and Enfield 2011; Lee et al. 2013; Barrett and Gensini 2013).

In the current study, a physical tornado climatology (comparing tornado counts, tornado day counts, and destruction potential between ENSO phases) is presented in section 3. Section 4 describes a dynamic climatology relating El Niño–La Niña to synoptic-scale atmospheric factors and processes fostering the development of tornado outbreaks (i.e., surface cyclones, tropospheric jet streams, static instability, tropospheric moisture content, and atmospheric geopotential height troughs). Conclusions of this study and the

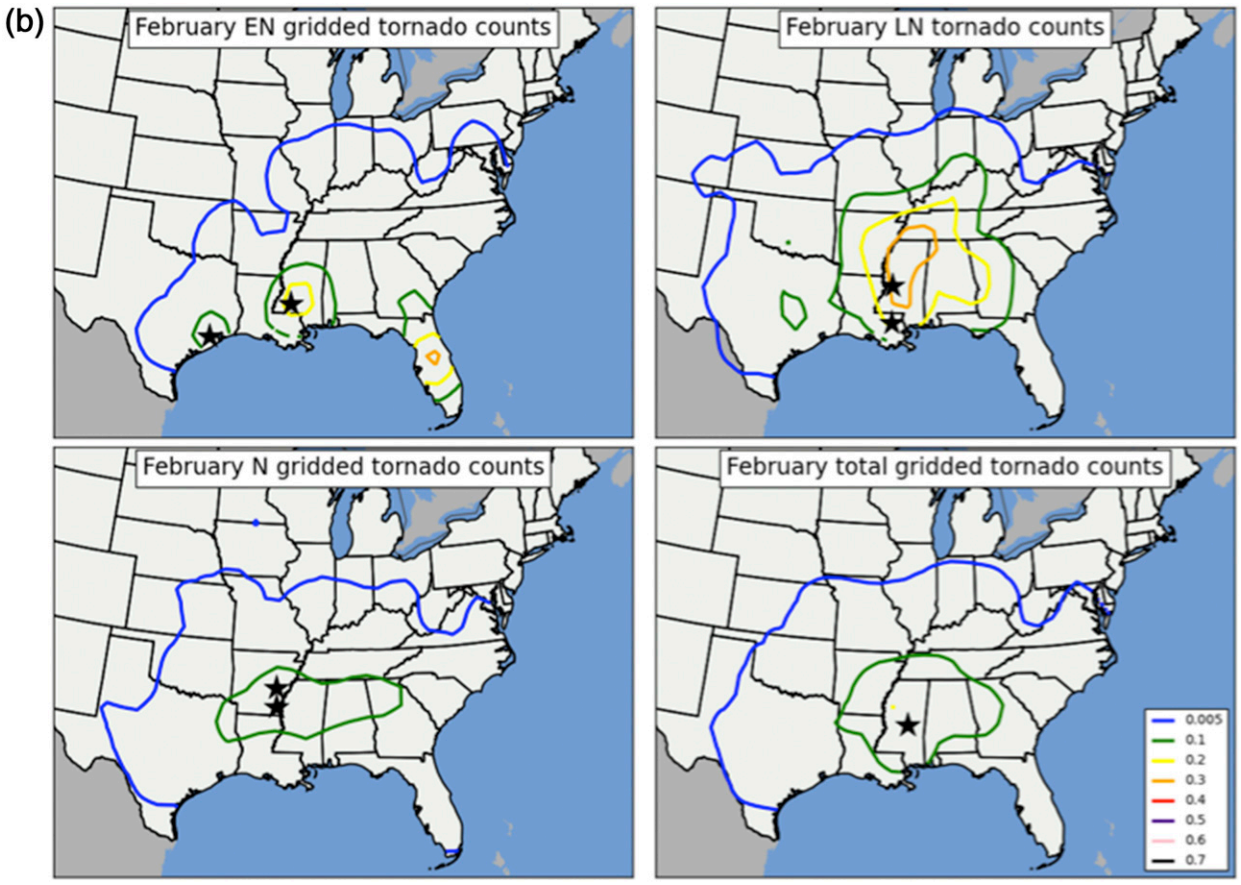

FIG. 3. (*Continued*)

implications for seasonal tornado forecasting are discussed in section 5.

2. Data and methods

a. Physical tornado climatology

A substantive task for creating the physical tornado climatology involved identifying tornado ''outbreak'' days. This subset of tornado data comprises tornado ''days'' (defined as 24-h periods from 0600 to 0600 UTC, in which six or more tornadoes were observed in the United States east of the Rocky Mountains) using the NOAA/NWS/NCEP/Storm Prediction Center (SPC) tornado–severe thunderstorm database (Schaefer et al. 1980; Schaefer and Edwards 1999). This 24-h criterion was employed because tornado outbreak days imply organization and influence by synoptic-scale atmospheric conditions that can in turn be influenced by larger, more global-scale atmospheric components. This outbreak criterion was alluded to and utilized in previous studies of tornado outbreaks (Pautz 1969; Galway 1975, 1977; Brooks et al. 2003; Schneider et al. 2004; Doswell et al. 2006). January to March periods of tornado day activity were an initial focus of the study, although April tornado days were included to examine several damaging, historic outbreaks (e.g., 11 April 1965 Palm Sunday outbreak; 3 April 1974 Super Outbreak) while also assessing continued teleconnections between El Niño–La Niña and atmospheric patterns in the United States beyond boreal winter.

The gridded tornado counts for the physical tornado climatology (Fig. 1) were constructed by first defining a basic 1° latitude by 1° longitude grid across the entire continental United States east of the Rocky Mountains, with each cell defined by a full degree of latitude and longitude. If a tornado path extended over distances greater than or equal to ~1.6 km (i.e., 1 mi) a set of latitude–longitude points was calculated for every 1.6 km of the tornado track. A count was then kept for each time a tornado track initially touched down on the grid and then subsequently crossed a parallel or meridian into a new grid cell. The process of defining the grid was repeated for several quantities used to gauge tornado activity: gridded tornado day counts and gridded DPI (Thompson and Vescio 1998, Doswell et al.

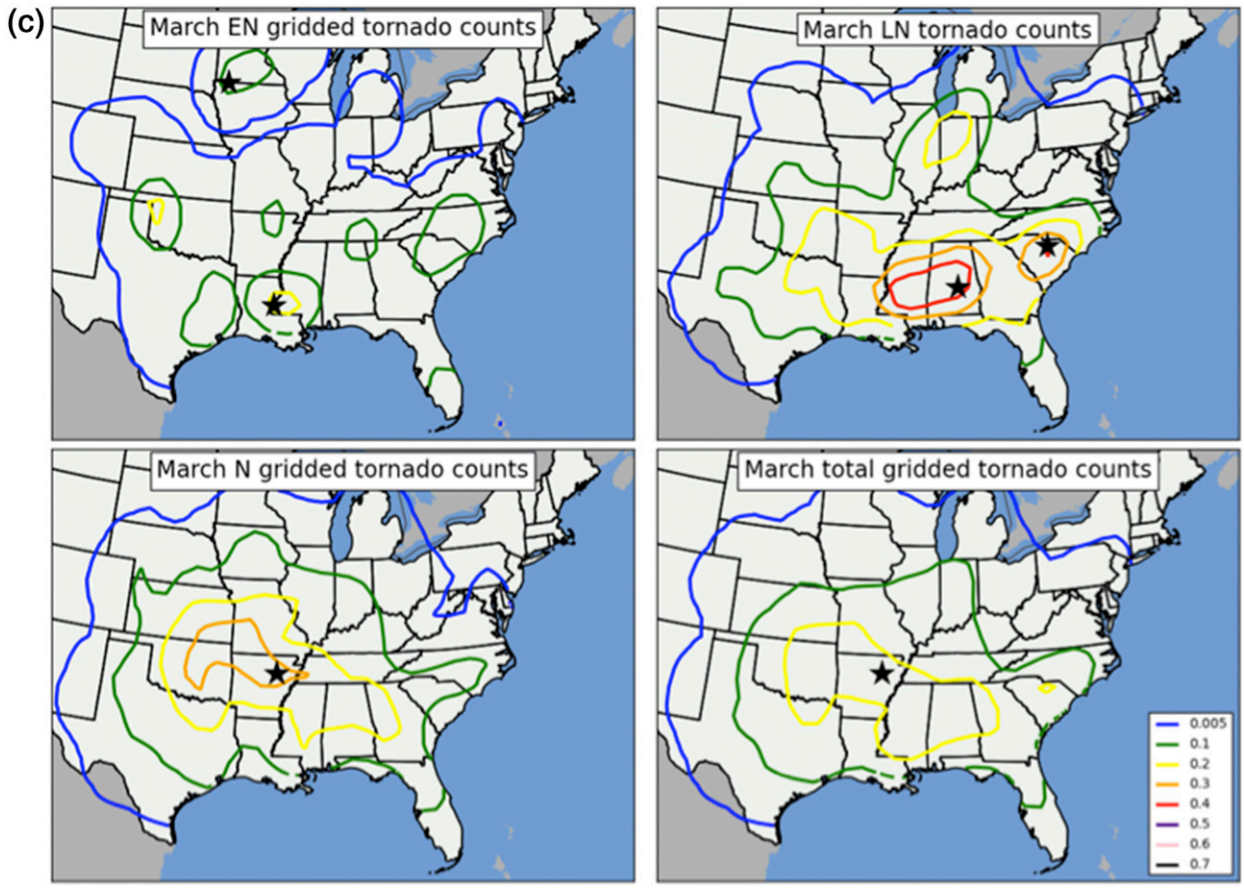

FIG. 3. (*Continued*)

2006). This gridding process is an enhancement over other spatial analyses of tornadoes because these gridded counts incorporated entire tornado tracks, whereas previous studies often utilized initial touchdown points (e.g., Kelly et al. 1978; Bove 1998; Brooks et al. 2003). The present approach enables (i) a more comprehensive spatial assessment of tornado locations across entire tracks, which is particularly helpful for longer-tracked tornadoes; and (ii) a more accurate assessment of potential impact in localized areas along the entire tornado track. The use of gridded DPI is particularly helpful in this regard, as it highlights areas historically prone to strong/violent long-tracked tornadoes in outbreaks more clearly than simple gridded tornado counts (Fig. 2).

In instances where climatologies were assessed for potential influences from ENSO, a definition largely similar to the CPC's definition of an ENSO event was utilized, with one key difference. Rather than using 3-month averages of sea surface temperature anomalies in the Niño-3.4 region (5°N–5°S, 170°–120°W), individual monthly sea surface temperatures in the Niño-3.4 region were used, with similar 0.5°C thresholds for defining an ENSO event, as already identified by CPC. This definition permitted a more direct comparison of monthly SST anomalies with monthly gridded tornado counts, tornado day counts, and destruction potential as described above, with a greater time resolution (monthly) than that of Cook and Schaefer (2008) (seasonal).

b. Dynamic tornado climatology (involving synoptic-scale atmospheric features associated with tornado outbreaks)

The climatology of synoptic-scale atmospheric features (i.e., surface cyclones, geopotential height troughs, lower- and upper-tropospheric jet streams, static instability, etc.; Table 1) presented here was based on composites derived from the NCEP–NCAR reanalysis dataset (Kalnay et al. 1996). This global dataset is defined on a 2.5° longitude by 2.5° latitude grid with 28 vertical levels. The domain used within this dataset encompasses the continental United States in a region bounded by 130° and 67.5°W and 25° and 50°N. A domain of this size allowed the aforementioned synoptic-scale features to be readily identified. Five variables from the reanalysis were used to create the atmospheric composites: geopotential height/sea level pressure,

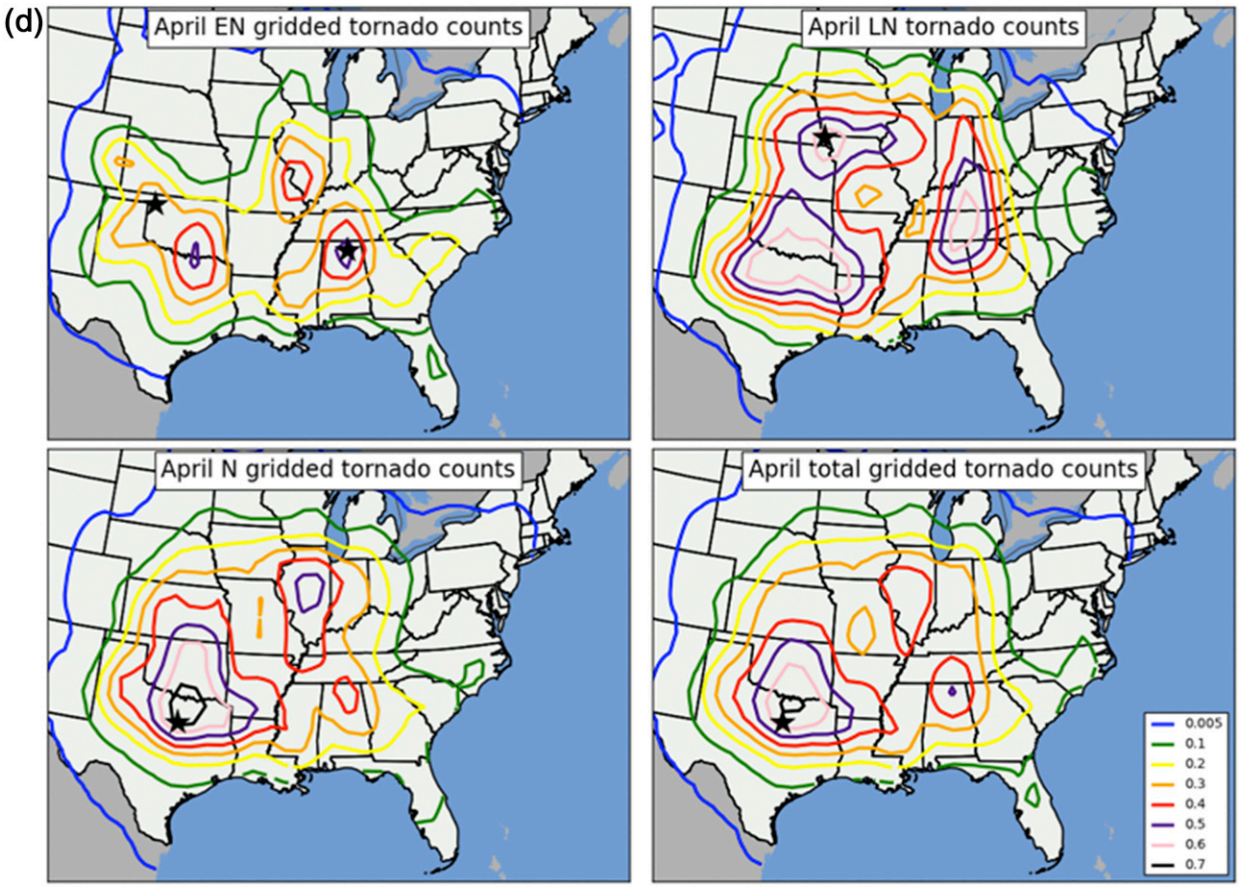

FIG. 3. (*Continued*)

temperature, relative humidity, the *U*-component wind, and the *V*-component wind at five different atmospheric pressure levels (surface, 850, 700, 500, and 300 hPa). Composites of the lifted index (Galway 1956) and column-integrated water vapor, often referred to as precipitable water, were created also to compare the presence of statically unstable warm sectors and the presence of moisture with the outbreak dataset.

TABLE 3. January–April 1950–2010 tornado frequency in outbreaks (as defined in section 1) east of the Rocky Mountains. Outbreaks are binned and then tallied according to concurrent ENSO phase.

	January			February			March			April		
	EN	LN	N	EN	LN	N	EN	LN	N	EN	LN	N
Tornadoes on outbreak days	221	412	160	151	418	323	205	788	1492	842	1614	3120
Tornadoes per number of months in each ENSO phase	10.52	19.62	8.42	11.62	23.22	10.77	20.50	46.35	43.88	69.67	100.88	94.18
Tornado outbreak days	23	21	12	17	36	30	20	68	100	63	113	214
Outbreak days per number of months in each ENSO phase	1.10	1.00	0.63	1.31	2.00	1.00	2.00	4.00	2.94	5.25	7.06	6.48
Tornadoes rated F/EF2 or greater	48	107	74	43	148	114	38	213	556	223	611	818
F/EF2+ tornadoes per number of months in each ENSO phase	2.29	5.10	3.89	3.31	8.22	3.80	3.80	12.53	16.35	18.58	38.19	24.79
Tornadoes rated F/EF4 or greater	2	3	5	1	12	4	1	12	47	19	70	63
F/EF4+ tornadoes per number of months in each ENSO phase	0.10	0.14	0.26	0.08	0.67	0.13	0.10	0.71	1.38	1.58	4.38	1.91
No. of months in each ENSO phase	21	21	19	13	18	30	10	17	34	12	16	33

TABLE 4. Seasonal evolution of DPI in tornado outbreaks east of the Rocky Mountains binned into separate phases of ENSO.

	January			February			March			April		
	EN	LN	N	EN	LN	N	EN	LN	N	EN	LN	N
Total DPI	214	896	279	137	2317	788	586	2350	7567	3882	7738	9543
Total kinetic energy (terajoules; FE15)	122.8	456.4	151.9	89.6	1080.2	398.5	267.5	1170.3	3557.6	1878.9	3531.8	4779.3
Avg cumulative DPI per tornado outbreak	9.32	42.64	23.25	8.04	64.37	26.28	29.30	34.56	75.67	61.62	68.48	44.18
Avg DPI per tornado in tornado outbreak	0.97	2.17	1.74	0.91	5.54	2.44	2.86	2.98	5.07	4.61	4.79	3.06
Avg cumulative path length per tornado outbreak	40.05	105.68	55.87	43.92	84.18	57.23	29.84	59.70	99.60	68.17	100.05	69.25
No. of outbreaks with DPI above 25	2	8	4	3	16	8	2	16	43	18	38	63
No. of outbreaks with DPI above 50	1	5	3	0	10	6	1	9	28	12	21	43

Reanalysis data for all outbreaks were available four times per day at 0000, 0600, 1200, and 1800 UTC. To determine the appropriate time of day for our analyses, an average of the start time for each tornado on a tornado outbreak day was calculated. The reanalysis time closest to the average of the start times of the individual tornadoes was utilized to determine the set of atmospheric conditions most representative of the

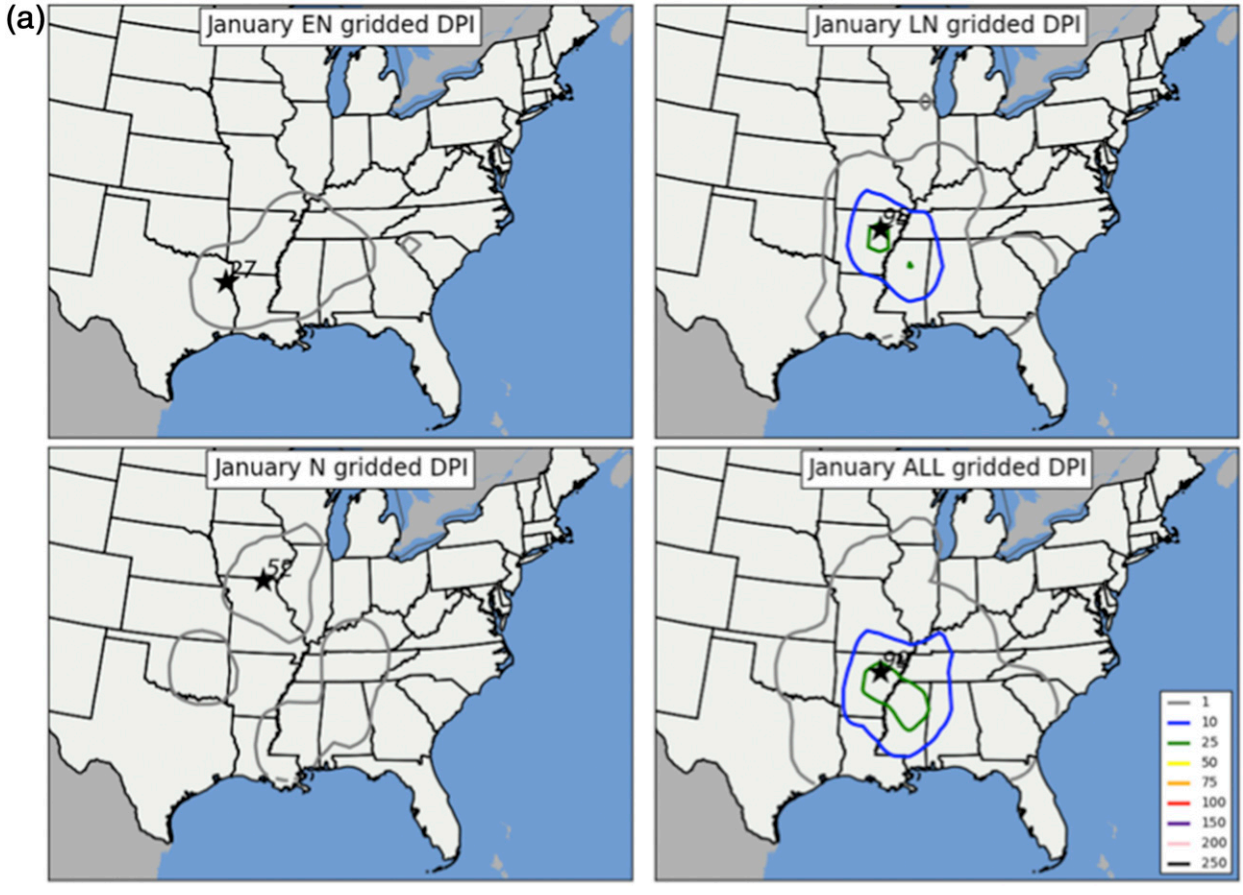

FIG. 4. Contour plots of gridded DPI values in El Niño, La Niña, neutral, and all (a) January, (b) February, (c) March, and (d) April tornado outbreaks from 1950 to 2010. Stars and associated contour-scale numbers indicate locations and numbers of the maximum DPI.

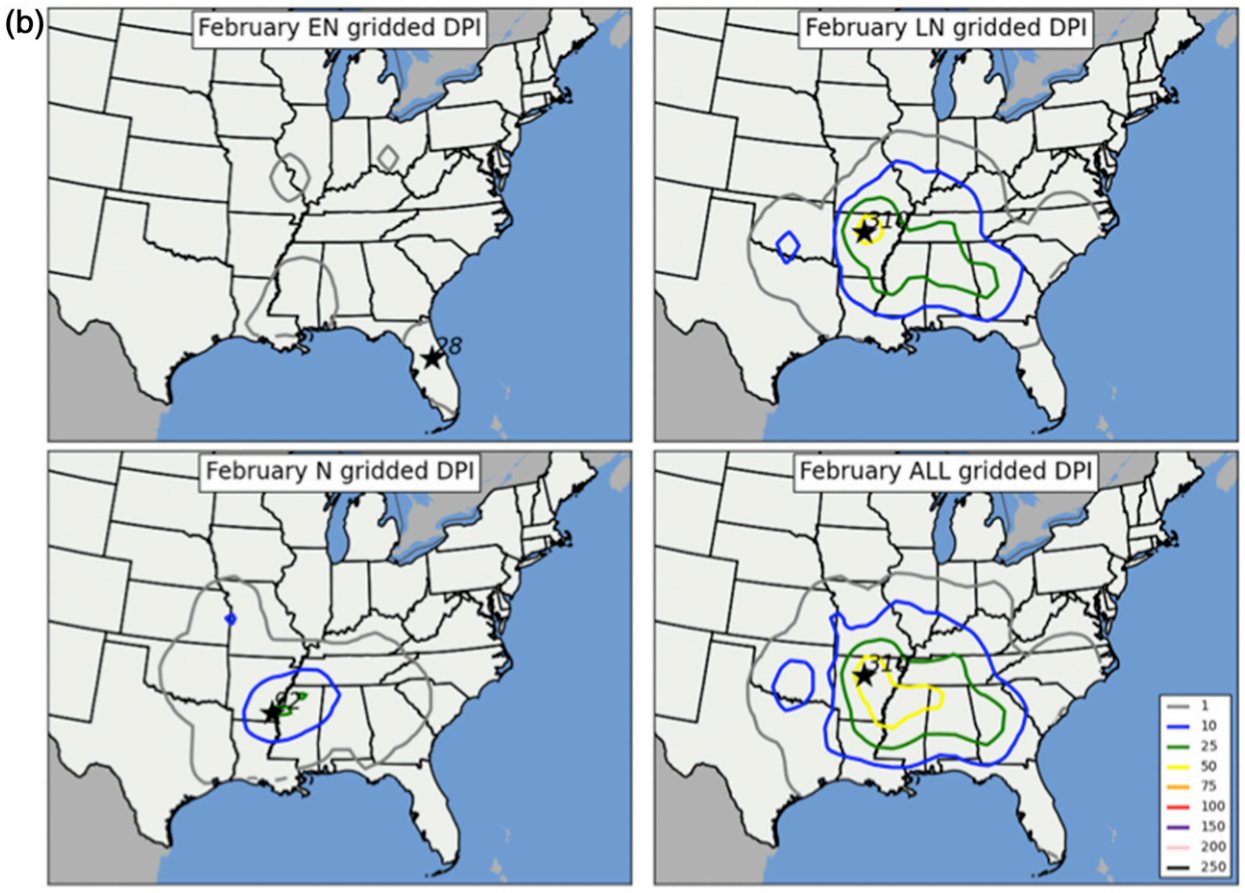

FIG. 4. (*Continued*)

tornado outbreak day. Frequently, this necessitated the use of 0000 UTC reanalyses, because start times for tornadic outbreaks generally occurred between 1200 and 1900 CDT (1800–0100 UTC).

An S-mode principal component analysis (PCA) (Richman 1986) was utilized to create composites of the synoptic-scale atmospheric conditions associated with tornado outbreaks to allow an analysis of intraseasonal shifts of tornado outbreaks from January through April, and to determine ENSO-related influences on location and character of the outbreaks. Such an approach allowed for identification of the relevant spatial anomalies in atmospheric fields near the time of individual outbreaks and also to provide an objective mechanism for compositing multiple events containing similar spatial anomalies. The method for creating composites of multiple outbreaks was adapted from Richman and Lamb (1985), who analyzed loading patterns based on intercorrelations between individual stations then addressed the use of ''principal component score time series'' as a basis for selecting individual cases for specific comparison. In the present study, analysis fields from individual outbreaks that met a PC score threshold of 1 were averaged to create a mean composite field. Because loadings are spatially oriented and the relationship between principal component scores and loadings is linear by definition, maxima (or minima) in composite fields often exhibited a close relationship to the locations of maximized loadings. Readers are referred to Richman and Lamb (1985), Richman (1986), and Montroy et al. (1998) for more detailed discussions of the PCA technique.

Although a PCA approach is widely utilized in the atmospheric sciences, this study is believed to be the first of its kind to create a climatology of synoptic-scale atmospheric features associated with tornado outbreaks during the January–April time frame to assess ENSO-related influences on this climatology. Other components of the analysis technique include statistical significance tests to determine whether temporal and spatial shifts in tornado activity are related to changes in ENSO patterns that are revealed using the aforementioned compositing analysis. Bias-corrected, accelerated confidence intervals (BCa CIs) were created for specific

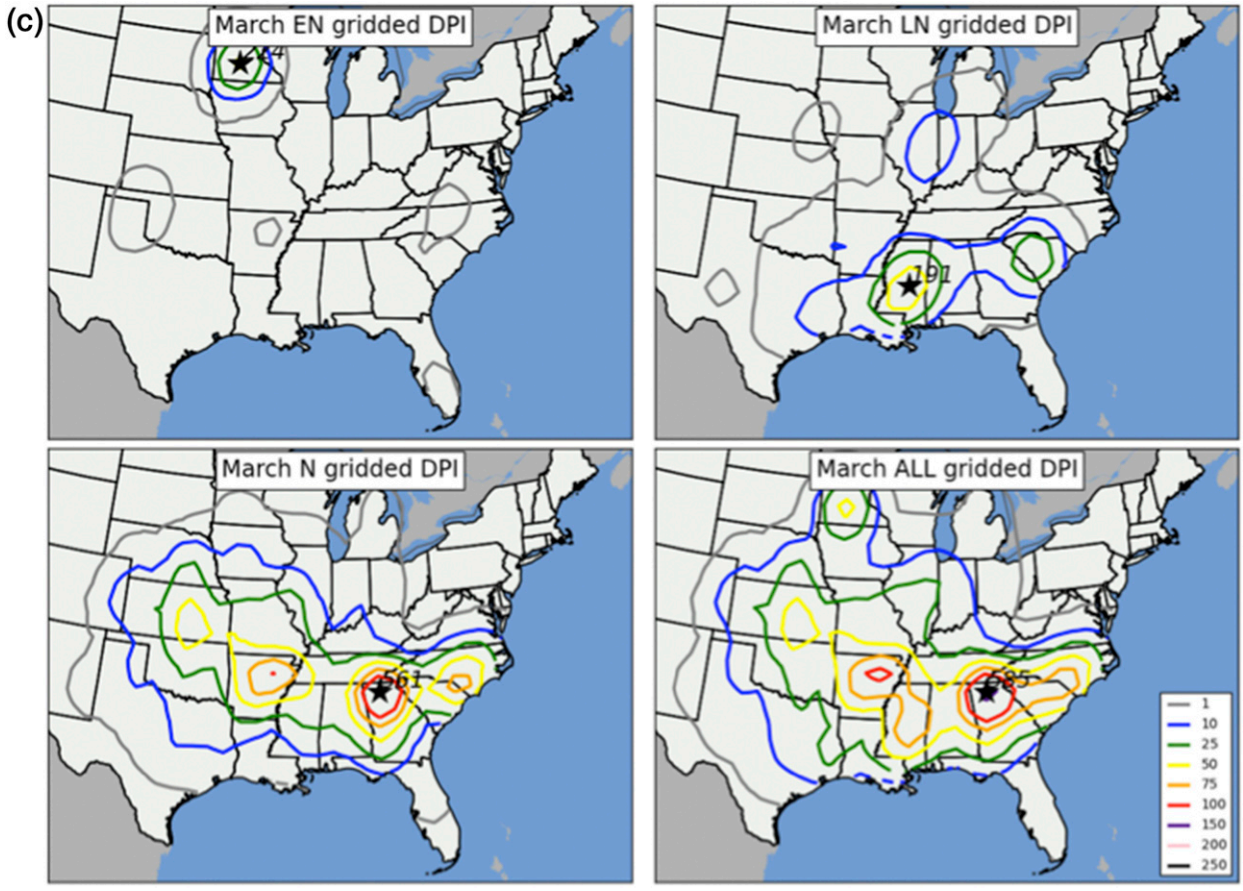

FIG. 4. (*Continued*)

regions within the analysis domain to conduct statistical significance tests of the findings (Efron and Tibshirani 1993; Dixon et al. 2011).

3. Possible influences of ENSO on the climatology of January–April tornadoes

To diagnose the impact of ENSO on tornado outbreak activity and to facilitate a comparison of tornadic outbreaks occurring in El Niño, La Niña, and neutral ENSO conditions, gridded tornado counts were normalized by the monthly frequency of occurrence for each particular ENSO phase during 1950–2010 (Table 2). Typically, the seasonal variation of tornado activity (Figs. 3a–d) exhibits an increase in the number of events and a westward and northward expansion of activity as the season progresses from January through April, with activity concentrated across parts of the Deep South in January–February and moving westward to the southern and central Great Plains in April.

The extent of the increased activity and its geographical expansion vary significantly between the El Niño tornado outbreaks and those occurring during neutral and La Niña phases. The patterns in Figs. 3a–d suggest that tornado activity during El Niño months occurs farther south than in other ENSO phases, with the most frequent occurrence of tornado outbreaks during El Niño taking place in eastern Texas and Mississippi from January to March except for an outlier outbreak in southern Minnesota on 29 March 1998. In contrast, La Niña tornado activity occurs more frequently north of those areas during that same time period, with maxima in central Arkansas and tornado outbreaks occurring as far north as Missouri, southern Illinois, and far southern Indiana in January and as far north as Nebraska and Michigan in March. Even larger differences between El Niño and La Niña appear over the central and northern Great Plains and eastward into Ohio in April (Fig. 3d), with increased tornado activity in La Niña years. The highest tornado counts occur during neutral months, but this difference is at least partially attributed to the higher frequency of monthly neutral ENSO events (Table 2), which occur nearly twice as frequently as El Niño months, particularly during February, March, and April.

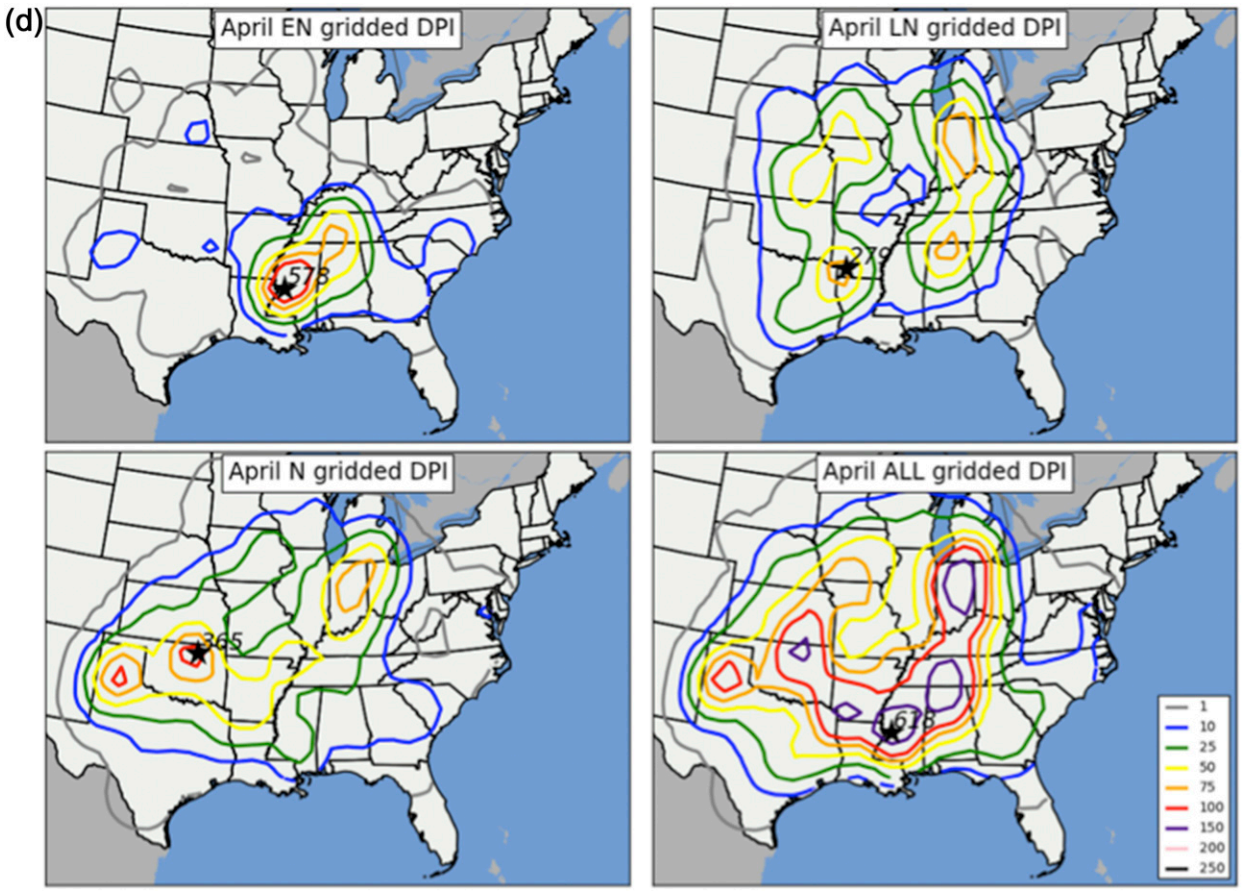

FIG. 4. (*Continued*)

Generally speaking, tornado outbreak activity is less frequent during El Niño conditions in the continental United States east of the Rocky Mountains relative to La Niña and neutral conditions (Table 3). Tornadoes on outbreak days during La Niña conditions in January and February substantially outnumber tornadoes occurring in other phases despite the fact that only 18 months were classified as La Niña in February (as compared with 30 neutral February months; Table 3). After normalizing by the frequency of ENSO classifications by month, it is found that January–February La Niña tornadoes occur with approximately twice the frequency of those occurring during El Niño conditions. This discrepancy is smaller in March and April, although tornadoes remain more frequent in La Niña and neutral phases than in El Niño phase. The occurrence of more frequent events during La Niña relative to El Niño conditions also applies to the tornadoes rated as strong (F/EF2 or greater) and violent (F/EF4 or greater), although smaller sample sizes for these metrics are more limited. These results are consistent with those of Cook and Schaefer (2008), who found that tornado activity in La Niña and neutral phases were more frequent in the entire continental United States from January to March 1950–2003. These results are also consistent with the results of Muñoz and Enfield (2011) and Kellner and Niyogi (2014) despite the more limited regional scope addressed in each of those investigations.

Tornado outbreak days were similar in frequency in El Niño and La Niña phases during January but more frequent in La Niña during February and more frequent during neutral conditions in March and April. This finding differs from Cook and Schaefer (2008) for two reasons: 1) the current study utilized month-to-month analyses as opposed to tornado activity analyzed for an entire seasonal period (January–March); and 2) ENSO events were gauged using an average Niño-3.4 SST anomaly spanning multiple months in the previous study, whereas the current study classifies an ENSO event based on the Niño-3.4 SST anomaly concurrent with the month being analyzed. In several years of the current study, Niño-3.4 SST anomalies indicated weak El Niño conditions in January that weakened even further in neutral conditions in February. As a result, El

Niño conditions identified via the definitions for ENSO outlined in section 2a occur in January more often than in any other month of the study.

An analysis of DPI, which provides information about the intensity and longevity of tornadoes in outbreaks, also reveals that stronger, longer-lived tornadoes in outbreaks are observed during La Niña conditions, especially in January and February (Table 4). During January and February La Niña, the average DPI per tornado outbreak (42.6 and 64.4) is dramatically higher than in outbreaks occurring in January and February El Niño (only 9.32 and 8.04, respectively). Additional metrics for comparing intensity of outbreaks (Table 4) clearly illustrate the disparity in destruction potential between El Niño and La Niña tornado outbreaks. Analyzing DPI values permits a more detailed assessment of tornado strength within outbreaks than in previous studies relating ENSO phases to tornadoes, while the use of total kinetic energy (Fricker and Elsner 2015, hereafter FE15) is also provided for comparison.

However, the abovementioned trend of stronger La Niña tornado outbreaks is far less pronounced in March and April. Neutral events tend to contain higher DPI in March based on almost all intensity metrics listed in Table 4. Although the differences in DPI per tornado outbreak in March El Niño and March La Niña are smaller than in the two prior months, the number of tornado outbreaks contributing to the higher DPI average in March El Niño is far less than the number of outbreaks contributing to the DPI average in March La Niña. This finding suggests that only a limited number of outbreaks with very high DPI values are contributing to the high average DPI in March El Niño tornado outbreaks. It also suggests that tornado outbreaks are generally more frequent with progression toward spring, suggesting that distinguishing a few additional outbreaks (as a function of ENSO) becomes more of a challenge. A similar conclusion can be made for April El Niño tornado outbreaks when compared with April La Niña tornado outbreaks; a smaller number of outbreaks that occur in April during El Niño phase contribute to the high average cumulative DPI per tornado outbreak when compared with April La Niña tornado outbreaks.

The strongest tornado activity during the El Niño phase (obtained from the spatial evolution of DPI with time) is consistently focused across the southern United States in all months of the study (Figs. 4a–d). DPI values in El Niño conditions are consistently small across the entire United States east of the Rocky Mountains until March, when a supercell spawned a few strong-to-violent tornadoes in southern Minnesota on 29 March 1998. Cook and Schaefer (2008) note that this tornado outbreak was a relative outlier when compared with other tornado outbreaks that occurred across the southern parts of the United States during El Niño. In April, larger values of DPI appear in the southern United States (particularly Mississippi), and much of that is the consequence of a single violent and long-tracked tornado with a pathlength of 149 mi and a maximum path width of 1.75 mi. That tornado was part of a larger outbreak of tornadoes that occurred in the Deep South on 24 April 2010. In contrast, tornadoes (and DPI maxima) occurred farther north during La Niña and neutral conditions in all months. The most striking example of this contrast is in April, where impactful tornado outbreaks struck areas from Nebraska and Kansas eastward to Indiana and western Ohio.

Despite the marked shifts in DPI patterns across the United States east of the Rocky Mountains, BCa CIs indicated statistically significant shifts in DPI in El Niño and La Niña conditions in only two areas, both during the month of April: in northern Kansas/far southern Nebraska and in northern Texas (not shown). In both statistically significant cases, tornado activity was more intense and influenced a larger area during La Niña conditions. The BCa CIs also indicate stronger tornado activity during El Niño conditions across the lower Mississippi valley in April. Although this finding contrasts with previous studies that indicated increased activity during La Niña, particularly in earlier months (January–March) (Cook and Schaefer 2008; Muñoz and Enfield 2011; Allen et al. 2015), this shift was not deemed statistically significant given the substantial overlap of the BCa CIs in both April La Niña and April El Niño conditions.

4. ENSO influences on the atmospheric conditions relevant to tornado outbreaks

a. January

ENSO-related shifts in low-level jet streams (located around 1 km AGL, or around 850 hPa) during January outbreaks are consistent with the observed shifts in January tornado activity presented in section 3, showing distinct northward and westward shifts in low-level jets and tornado activity within January La Niña outbreaks (Fig. 5). During January La Niña outbreaks, low-level jet streams in outbreaks are concentrated across the Tennessee and Ohio River valleys, with individual jet streams located as far west as Missouri and Arkansas during individual outbreaks. In contrast, low-level jet streams are located farther south and east (from Louisiana to the Carolinas) during the individual January El Niño outbreaks. These shifts are also observed in monthly averages of 850-hPa V-component wind primarily in the eastern two-thirds of the continental United States (Fig. 6); large

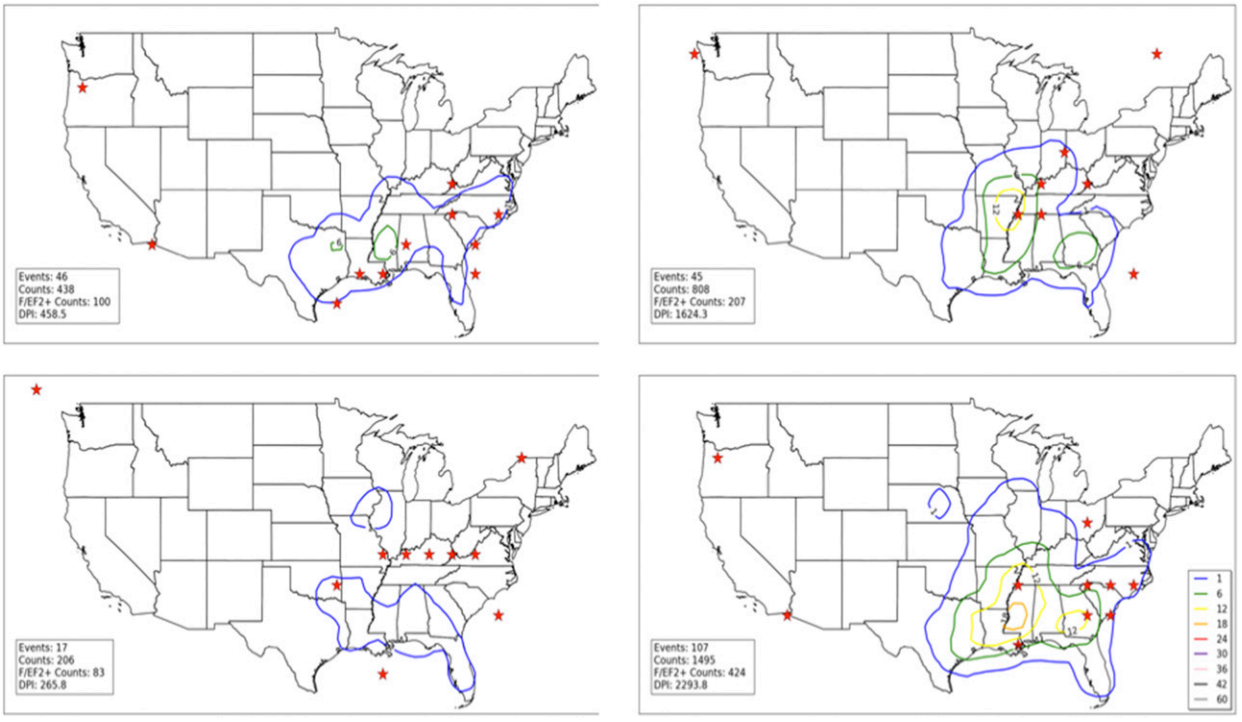

FIG. 5. Locations of maximum 850-hPa *V*-component wind (red stars) for (top left) all El Niño January, (top right) all La Niña January, (bottom left) all neutral January, and (bottom right) all January tornado outbreak 850-hPa geopotential height composites. Contours represent concentrations of tornado activity concurrent with events used to create composites. Tornado counts are on a 1° × 1° grid as described in section 2.

positive anomalies of 850-hPa *V*-component wind are located from northeastern Texas into western Arkansas during La Niña, suggesting that these shifts are also observed independent of individual tornado outbreaks.

ENSO-related shifts in convective instability maxima (indicated by the lifted index) also exhibits similar ENSO-related spatial shifts as those trends exhibited by low-level jet streams (Fig. 7). During January El Niño conditions, instability axes in outbreaks are located across areas adjacent to the Gulf of Mexico from Texas into Florida. During January La Niña conditions, instability in outbreaks is drastically decreased across much of Florida and southern Georgia but is increased along the middle Mississippi and Ohio River valleys, consistent with and explaining the increased tornado activity during January La Niña in those locations.

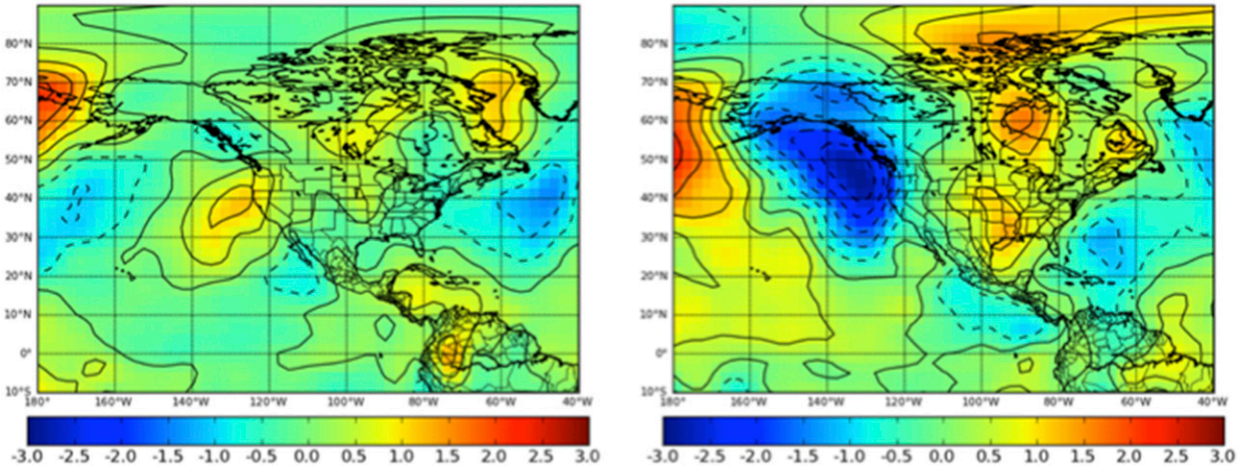

FIG. 6. Monthly anomalies of 850-hPa *V*-component wind ($m\,s^{-1}$) during January (left) El Niño and (right) La Niña conditions.

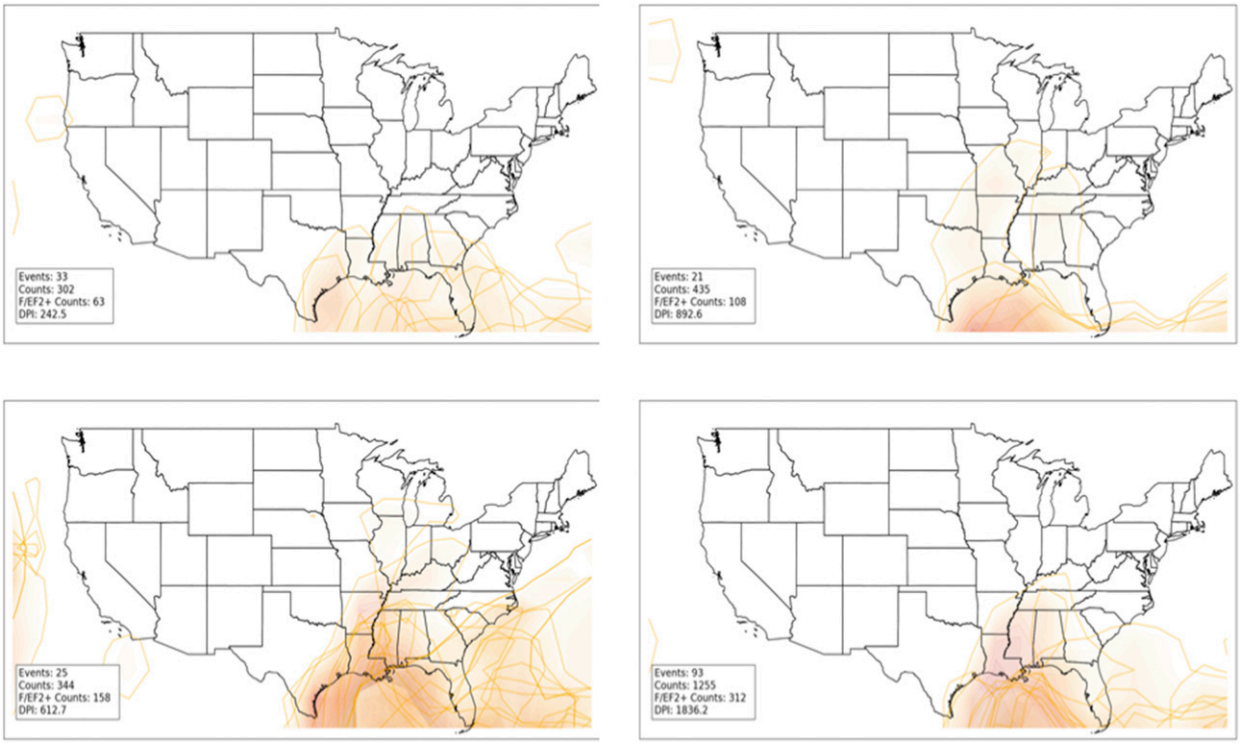

FIG. 7. Instability axes (noted by shaded regions where the lifted index < 0) in each composite during (top left) January El Niño, (top right) January La Niña, (bottom left) January neutral, and (bottom right) all January tornado outbreaks. Stars indicate locations of largest negative anomalies (departures from mean of all January tornado outbreaks) of the lifted index. Darker shading indicates stronger instability (i.e., lower lifted index).

Evidence of ENSO-related shifts in upper-level jet streams also is present during January outbreaks, although pattern shifts are less clear than the aforementioned low-level jets and instability axes (Fig. 8). Monthly averages of 300-hPa scalar wind fields indicate anomalous strong 300-hPa flow from the Pacific, through northern Mexico, and into Florida during January El Niño conditions. This shift in jet stream patterns is likely an extension of the southerly displaced jet stream influenced by ENSO, identified previously (Rasmusson and Mo 1993; Cook and Schaefer 2008; NOAA/CPC 2015; http://www.cpc.ncep.noaa.gov/products/analysis_monitoring/ensocycle/nawinter.shtml). Given the relationship between upper-level jet

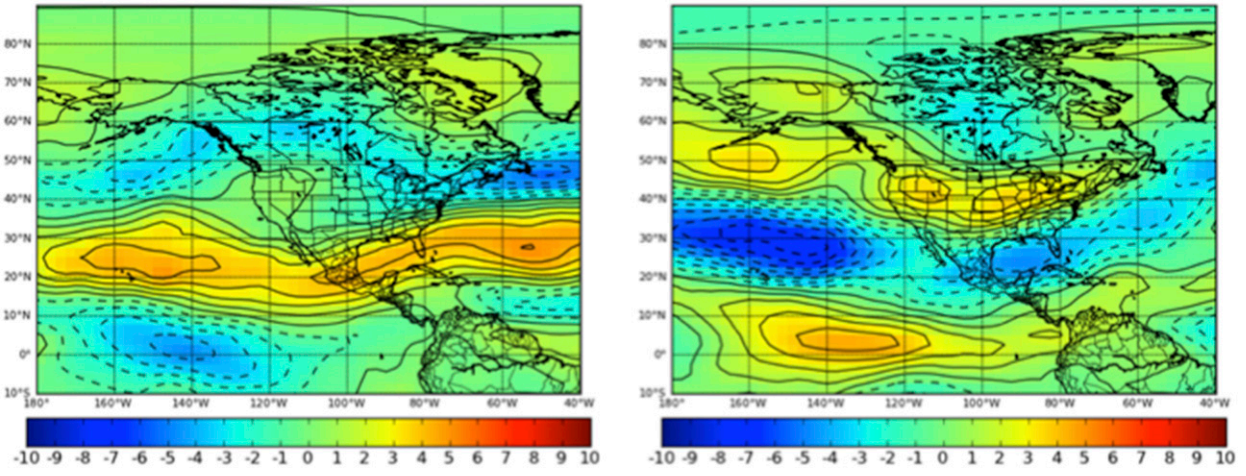

FIG. 8. As in Fig. 6, but for 300-hPa scalar wind (wind speeds).

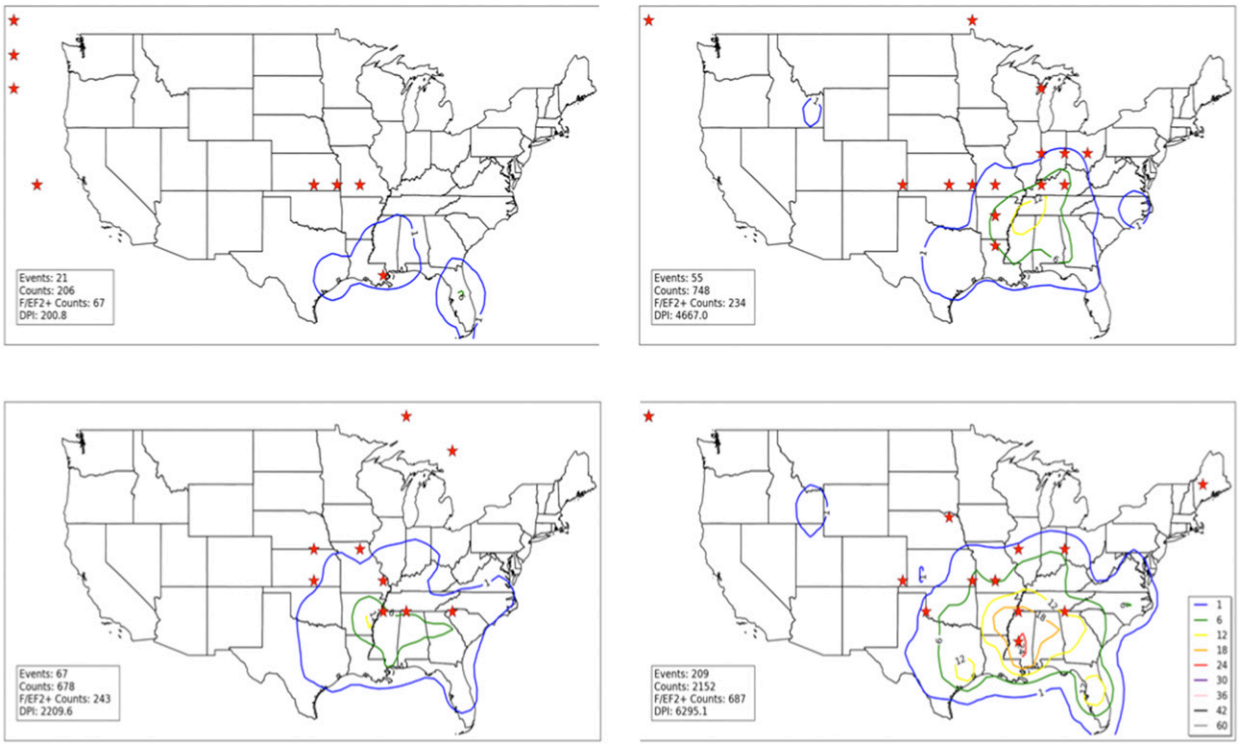

FIG. 9. Locations of minimum SLP (red stars) for (top left) all El Niño February, (top right) all La Niña February, (bottom left) all neutral February, and (bottom right) all February tornado outbreak SLP composites. Contours represent concentrations of tornado activity concurrent with events used to create composites. Tornado counts are on a 1° × 1° grid as described in section 2.

streams and synoptically driven low-level jet streams as described by Uccellini and Johnson (1979), it is plausible that the aforementioned southward displacement of the low-level jet streams is tied to this southward displacement of higher-altitude jet streams. The combined influence of southward shifts in low- and upper-level jet position, due to El Niño conditions, appears to create favorable conditions that likely contribute to the statistically significant decrease in tornado activity across the lower Mississippi valley.

Some conflicting results arise, however, when assessing upper-level jet streams in individual outbreaks. Rather than a clear southward displacement in upper-level jets indicated in monthly averages of 300-hPa scalar wind fields in Fig. 8, upper-level jets exhibit more variable behavior, with the only clear signal for decreased upper-level jet stream activity located in the Pacific Northwest during January El Niño (not shown). While no definite explanation is apparent for the differences between the behavior of upper-level jets from individual outbreaks and monthly means, this implies that jet stream positions within January outbreaks are more anomalous relative to the 300-hPa scalar wind fields during that month. Notably, subsequent months do not exhibit this behavior, and individual composites appear to be much more closely related to monthly 300-hPa anomaly fields of geopotential heights and wind fields.

b. *February*

ENSO-related shifts in the February climatology of synoptic-scale atmospheric features are generally consistent with the results outlined in section 3 that indicate more frequent tornado activity across the southern tier of the United States (particularly Mississippi) during La Niña conditions. Composites reveal a greater frequency of surface cyclones in outbreaks near the Great Lakes during La Niña conditions and a southward shift in surface cyclone frequency in one of the composites (over southeastern Louisiana) during El Niño (Fig. 9). This is consistent with Eichler and Higgins (2006), who indicated a greater frequency in surface cyclone storm track toward the western Great Lakes during winter La Niña conditions and across the Gulf of Mexico during winter El Niño.

Differences between 300-hPa jet streams during February El Niño and La Niña tornado outbreaks (Fig. 10) are far more striking than those identified in January El Niño and La Niña tornado outbreaks (described in section 4a). These jet streams are far more

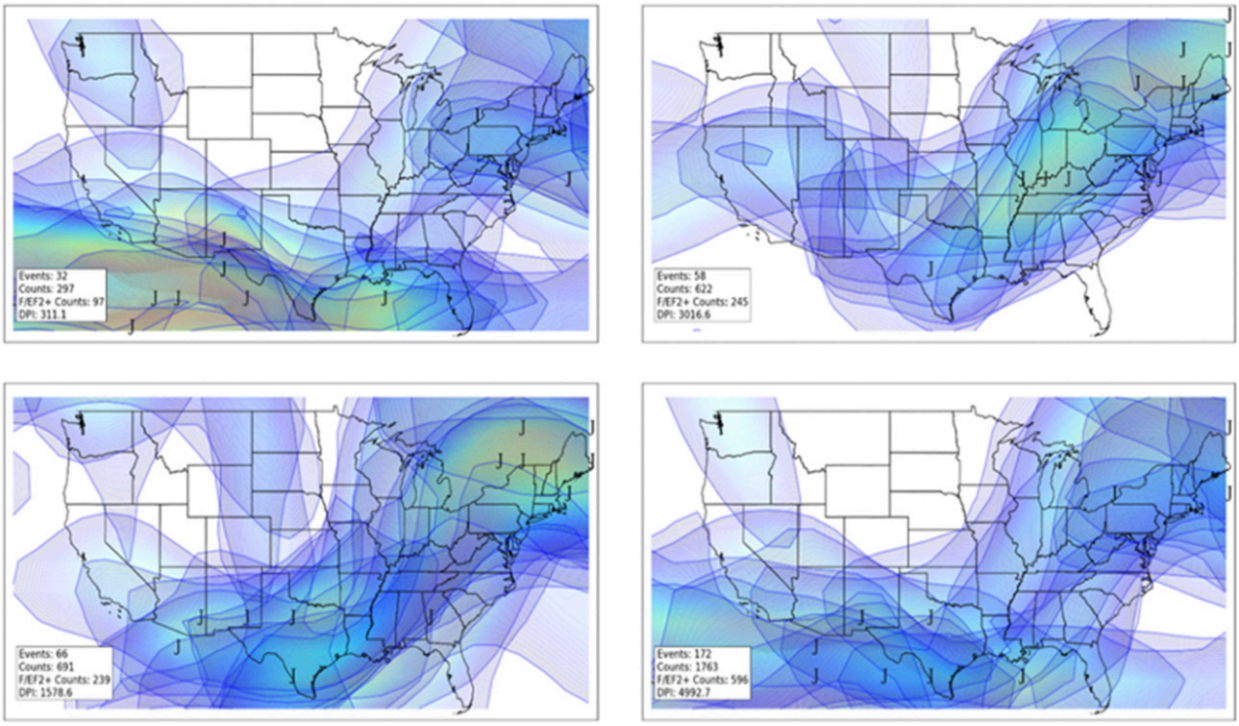

FIG. 10. The 300-hPa jet streams in individual composites of February (top left) El Niño, (top right) La Niña, (bottom left) neutral, and (bottom right) all outbreaks. Here, the letter J indicates jet stream wind maxima, while shaded areas indicate location of winds associated with individual jet streams of at least 70 kt (1 kt = 0.5 m s^{-1}). Lighter shading (yellow, red) indicates stronger winds.

intense and frequent during February El Niño outbreaks, extending from near Baja California eastward across the Gulf of Mexico. In contrast, upper-level jets are far more frequent and intense from near Arkansas northeastward to the northeastern United States and adjacent southeastern Canada. Monthly averages of 300-hPa wind fields (not shown) also indicate similar shifts, suggesting that these ENSO-related shifts are observed both during outbreaks and also within the mean state of the atmosphere. These jet stream shifts are consistent with several previous studies (Rasmusson and Mo 1993; Cook and Schaefer 2008; NOAA/CPC 2015) with regard to a southward displacement in mean surface cyclone track identified in Eichler and Higgins (2006) and also a southward shift in location of low-level jet streams shown in Fig. 11 (Uccellini and Johnson 1979). The southward shift in tornado activity (and the decrease in the lower Mississippi valley and increase in Florida) is also supported by these atmospheric shifts.

The distinct ENSO-related shifts that appear in surface cyclone locations, upper-level jets, and lower-level jets do not appear as strongly in the instability fields during February outbreaks (not shown). In those outbreaks, instability tends to be located mostly across the Gulf of Mexico and northward into the lower Mississippi valley. Only in February tornado outbreaks during neutral conditions does the instability extend farther northwest into Kansas and Missouri. In other February El Niño and La Niña outbreaks, instability extends northeastward into Kentucky and Tennessee. These results indicate that while instability is a necessary condition for tornado outbreaks, it alone is not sufficient for tornado outbreak development. Tornado outbreak activity appears to be more readily modulated by the dynamic processes associated with the low-level and upper-level jet streams.

c. *March*

March composites of sea level pressure (SLP) (Fig. 12) are not particularly conclusive in supporting the ENSO-related shifts in activity discussed in section 3. These composites indicate a surface low across southern Wisconsin associated with tornado outbreak activity across Illinois and Indiana. Other SLP minima indicated in composites across the Ohio–Tennessee River valleys and southern Appalachians support increased tornado activity in the southern United States from Alabama to the Carolinas. In El Niño March composites of SLP, minima are located from southern Colorado to Ohio, but tornado activity associated with

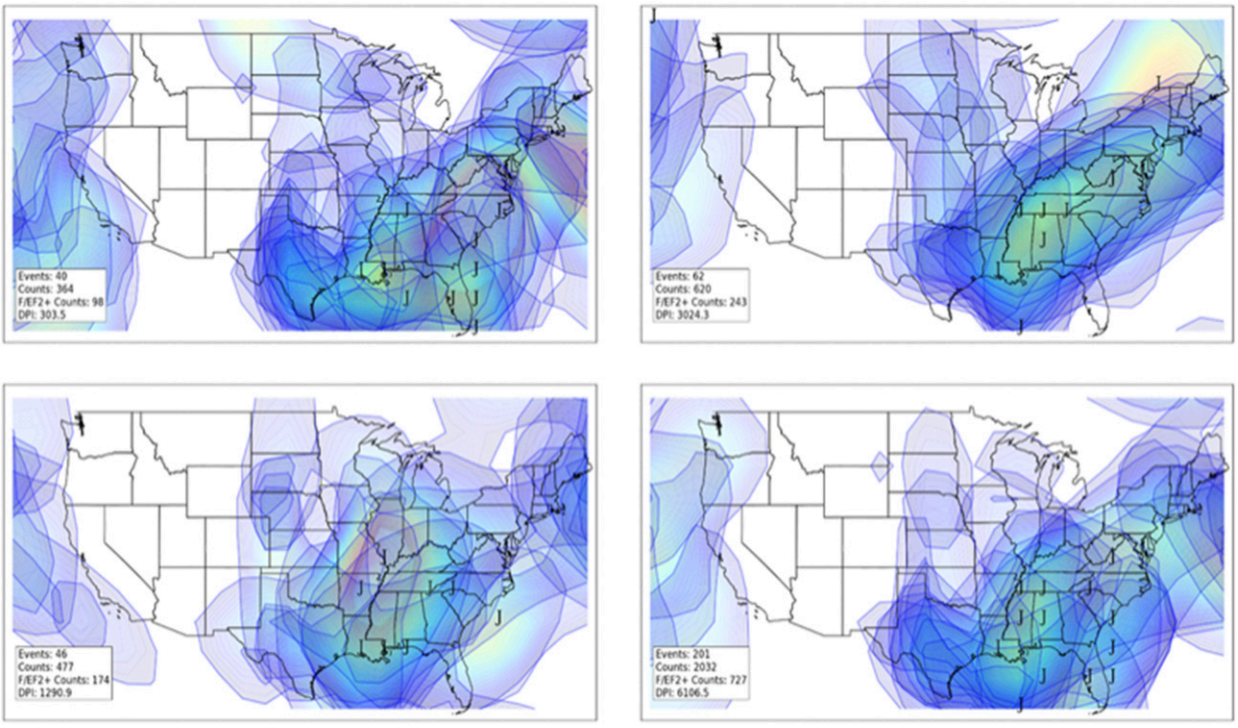

FIG. 11. As in Fig. 10, but for the 850-hPa jet streams. Shaded areas indicate location of winds associated with individual jet streams of at least 20 kt.

these minima is not nearly as extensive in the vicinity of those minima in La Niña March composites, suggesting the likelihood of additional atmospheric factors not shown in SLP composites that influence tornado activity.

In the upper levels, a more distinct, ENSO-related bimodal shift in upper-level jet streams is indicated in composites (Fig. 13), with a southwardly displaced jet stream noted in El Niño March tornado outbreaks across southern Texas, southern New Mexico, and Mexico consistent with results from outbreaks during February (section 4b). Monthly averages of 300-hPa scalar wind (and associated anomalies; not shown) are also consistent with this finding and indicate anomalously strong winds during El Niño across the eastern Pacific, Mexico, and Florida. During La Niña conditions, 300-hPa wind maxima in composites are found mainly across the southern Great Plains and also the northeastern United States. These shifts are consistent with the changes in the surface cyclone activity and low-level jet behavior and their impact on tornado activity. Similar impacts on surface cyclone activity and low-level jets have been previously observed and described in January (section 4a) and February (section 4b).

Substantial ENSO-related spatial shifts in instability fields are seen within composites of the lifted index during March tornado outbreaks. During El Niño outbreaks in March, areas of static instability are located across a large part of the United States, including the Pacific Northwest, southwestern United States, and Great Plains from the Gulf Coast to as far north as southeastern South Dakota. In contrast, instability is focused from the lower Mississippi valley northward to northern Indiana during La Niña March outbreaks. The static instability in some El Niño March outbreaks is inconsistent with the decreased tornado activity observed during El Niño March across those areas (particularly north of the central Great Plains eastward to the upper Midwest), suggesting that either 1) there is an absence of additional synoptic-scale atmospheric features necessary for the development of tornado outbreaks in those areas (i.e., lift and shear), or 2) smaller-scale atmospheric phenomenon not resolved by the present analysis (employing 2.5° by 2.5° reanalyses) are not supportive of tornado outbreak development in those areas.

d. April

April is the most active month of the study and contains several of the most distinct ENSO-related shifts, in both physical and atmospheric climatologies, of the entire study. Shifts in surface cyclone locations are noted

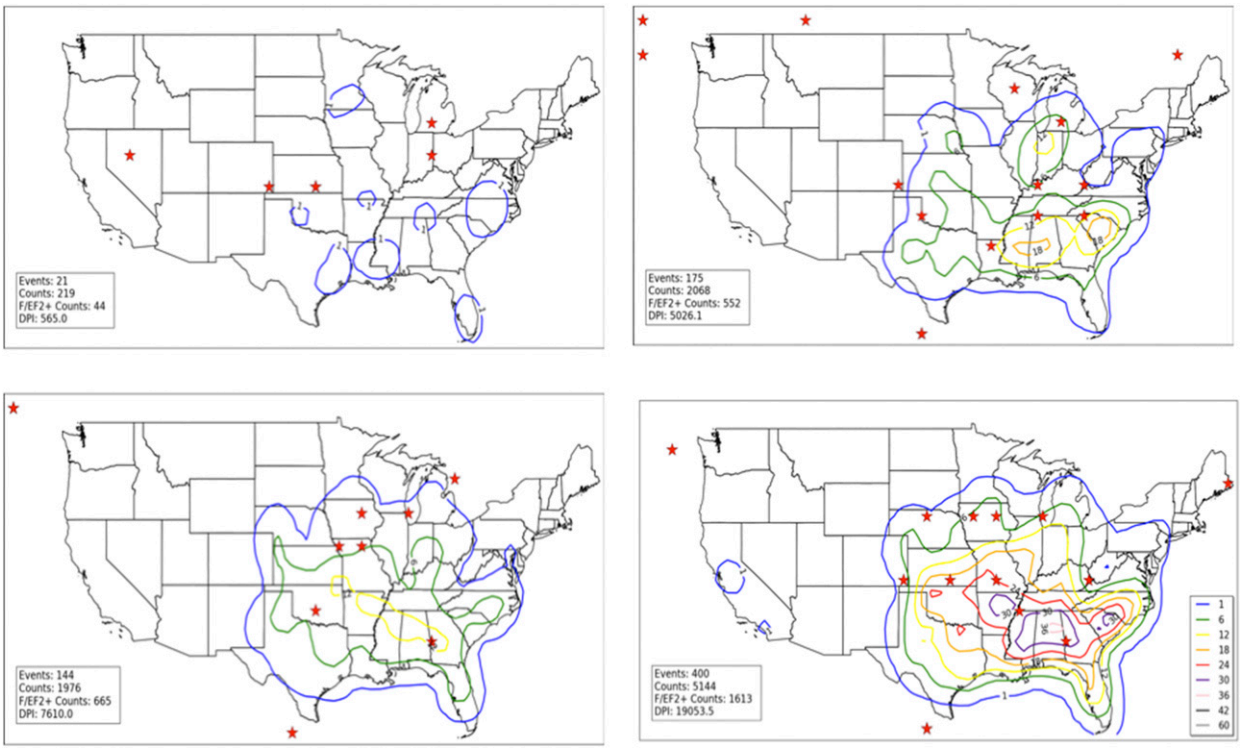

FIG. 12. As in Fig. 9, but for March.

in April composites of sea level pressure (Fig. 14), with focused surface cyclone activity in an area from Kansas northeastward to Wisconsin during La Niña conditions and a dearth of surface cyclones across the remainder of the United States during outbreaks. Low-level jet streams within individual tornado outbreaks also exhibit a distinct northward shift (not shown), and strongly anomalous 850-hPa meridional wind (Fig. 15) is also evident across the Great Plains during La Niña (likely indicative of more frequent southerly low-level jet formation across those areas). Instability within individual tornado outbreaks (Fig. 16) also exhibits a distinct northward shift during La Niña conditions in April. Each of these atmospheric shifts (both within individual outbreaks and monthly means) appears to be strongly tied to an overall increase in tornado frequency across the United States east of the Rocky Mountains during April La Niña conditions, with the most distinct shifts occurring in an axis from Nebraska eastward to Ohio. During El Niño conditions, surface cyclones within composites of outbreaks are displaced to the south (across Kentucky, southeastern Missouri, and Pennsylvania). Low-level jets exhibit similar behavior, and resultant tornado activity also exhibits a southward shift relative to April La Niña tornado outbreaks.

Although ENSO-related shifts in upper-level wind maxima (indicated by maximum 300-hPa wind in composites; Fig. 17) are less distinct than in the previous months, there are notable shifts involving the enhancement of the upper-level jet that has an impact on tornado outbreaks across the southern tier of the United States from Texas to Alabama. On a monthly time scale, some shifts in wind anomalies at 300 hPa as a function of ENSO are apparent (Fig. 18), particularly in the eastern Pacific east of Hawaii and also across Mexico. Geopotential height means (and departures) at 500 (Fig. 19) and 300 hPa (not shown) suggest favorable patterns for tornado outbreaks in the Great Plains because of 1) increased southwesterly flow aloft, just east of areas of negative geopotential height anomalies located over the intermountain west; 2) a synoptic-scale, low-level jet response due to increased southwesterly flow aloft and negative geopotential height anomalies west of the low-level jet axis; and 3) warm, moist advection due to the enhanced meridional synoptically driven low-level jet. It is noteworthy that a few of the larger outbreaks in the dataset that occurred east of the Rocky Mountains developed in particular geopotential height–jet stream configurations for classic tornado outbreaks that are favored during April La Niña patterns.

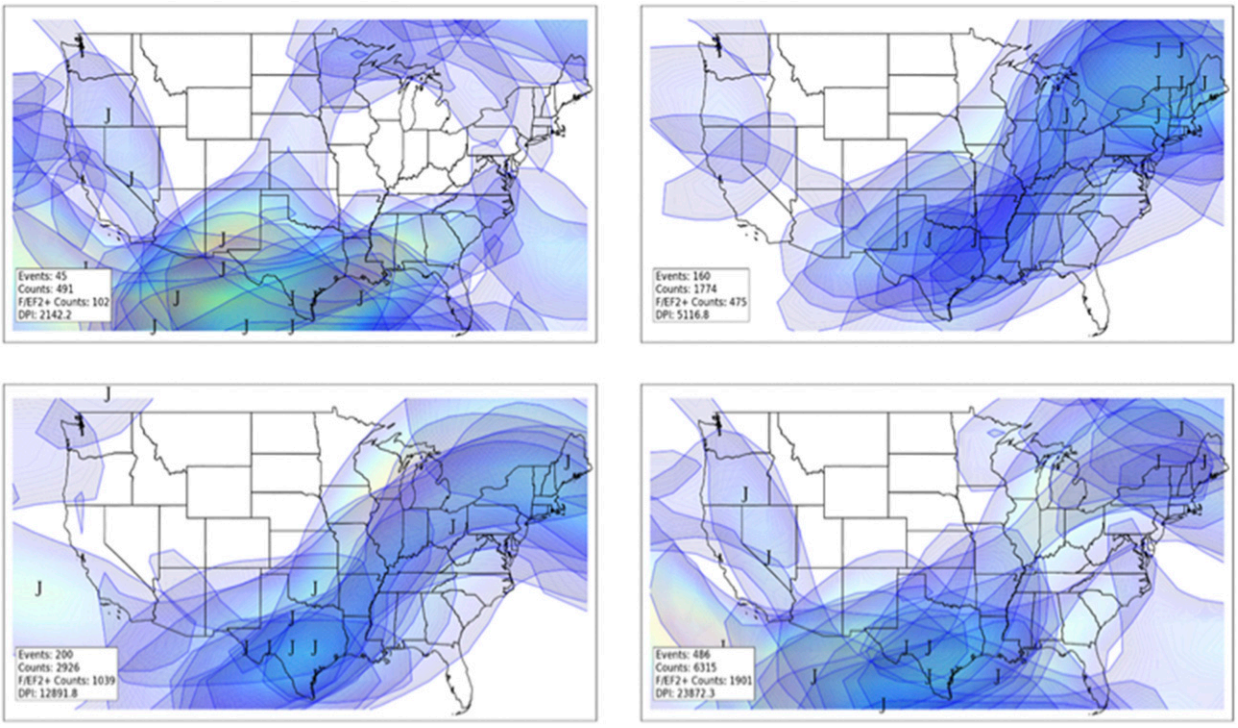

FIG. 13. As in Fig. 10, but for March.

5. Conclusions

The results of this study illustrate the changes in the climatology of tornado outbreaks as a function of ENSO. In each of the four months from January to April, tornadoes occur less frequently and at more southerly latitudes during El Niño conditions, with a distinct increase and northward extension of tornadoes in outbreaks that occur during La Niña conditions. Using normalized and gridded metrics for tornado outbreaks along with bootstrap resampling, ENSO-related shifts in the physical tornado climatology were found to be statistically significant.

The atmospheric climatology presented here extends beyond previous work by investigating the ENSO-related climatology of *individual* tornado outbreaks. These analyses further support the claim that synoptic-scale atmospheric conditions across the continental United States are influenced by ENSO and, in turn, affect the location of tornado activity. Some of these atmospheric features are more well known to be directly tied to ENSO (e.g., upper-level jet streams) than other features (e.g., surface cyclones, instability and moisture axes, and low-level jet streams). During El Niño conditions, upper-level jets were found to be abnormally strong and southwardly displaced, affecting the location of low-level jet formation, surface cyclone formation, and subsequent development of instability axes to foster a southward shift in tornado activity from January through April. During La Niña conditions, upper-level jets occur farther north, promoting development of low-level jet streams and instability axes farther north and west across the continental United States, thereby resulting in increased tornado activity farther north and west of the locations that experience more frequent tornado outbreaks in El Niño conditions (i.e., the Great Plains and western Great Lakes areas). Previous studies (Cook and Schaefer 2008; Muñoz and Enfield 2011; Lee et al. 2013; Allen et al. 2015; Sparrow and Mercer 2016) only considered monthly or seasonal averages to infer related shifts in tornado activity rather than considering individual outbreaks. Kellner and Niyogi (2014) did not consider any ENSO-related atmospheric shifts that would alter tornado activity.

The ENSO-related evolution of sea surface temperatures progresses slowly over time. Given the slow evolution of ENSO and its strong influence on Northern Hemispheric weather, often lasting for many months, the possibility exists for developing a seasonal tornado forecast indicating favored geographic regions for above- or below-normal activity based on ENSO phase.

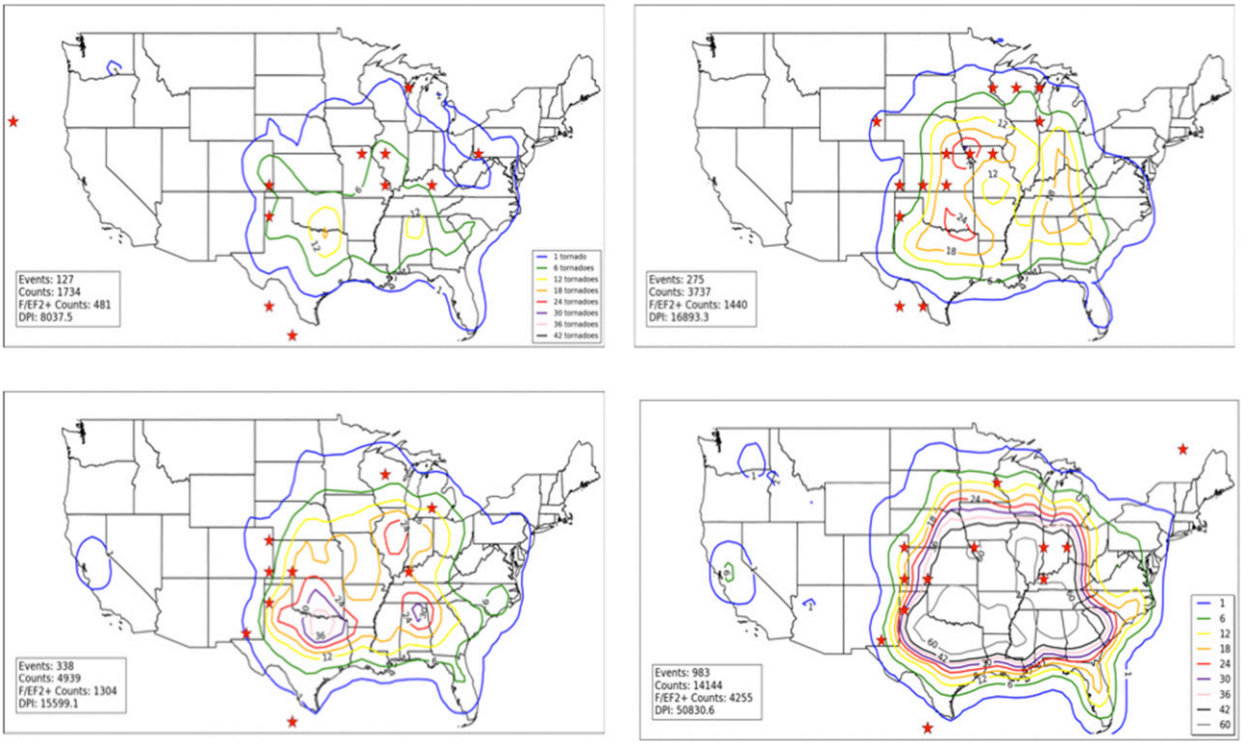

FIG. 14. As in Fig. 9, but for April.

The present study has the following implications for such an approach:

1) The direct and indirect influences of ENSO on synoptic-scale atmospheric features associated with tornado outbreaks and related influences on tornado activity have not been previously defined. In the present study, these relationships have been established not only on a seasonal or monthly averaged basis, as in previous studies, but also have been established for *individual* tornado outbreaks. As a consequence, the influence of ENSO on upper-level jet streams, low-level jet streams, and instability *within individual outbreaks* has become clearer.
2) The ENSO-related physical climatology tied to monthly variations and synoptic variability affords an opportunity to approximate the expected number of tornado outbreaks in *future* particular months or

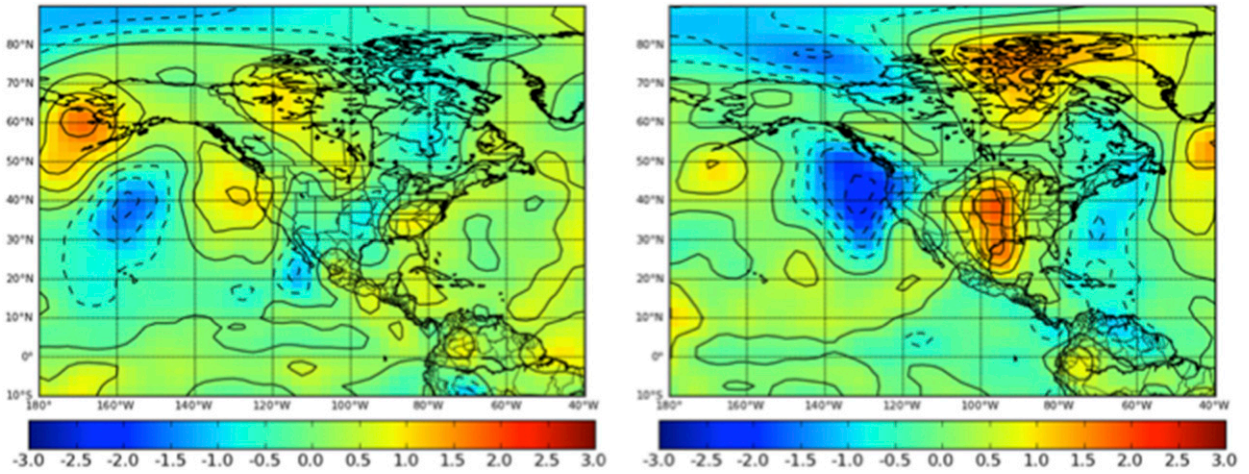

FIG. 15. As in Fig. 6, but for April.

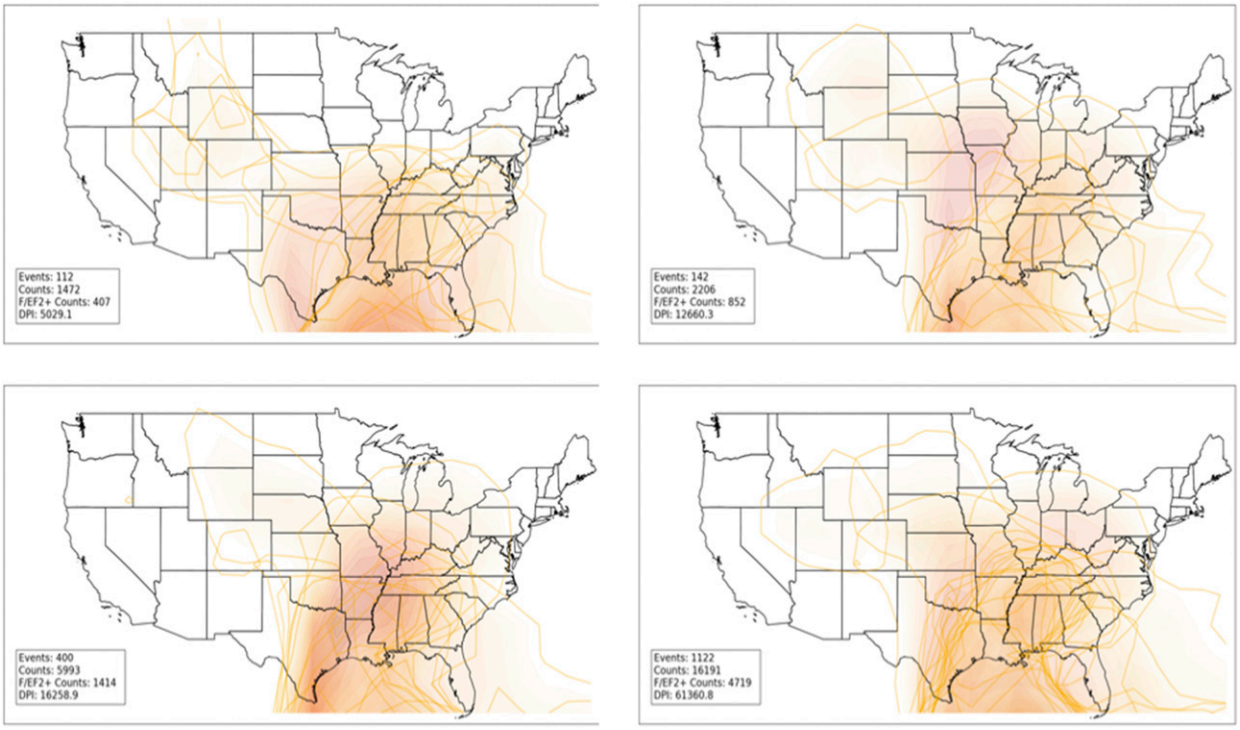

FIG. 16. Areas of negative lifted index in composites of individual April (top left) El Niño, (top right) La Niña, (bottom left) neutral, and (bottom right) all outbreaks.

seasons. Cook and Schaefer (2008) provided the foundation for this type of forecast, but the current study has presented a deeper, more detailed investigation into this type of forecast potential than previously available. The present approach included the systematic identification and inclusion of all individual January–April tornado outbreaks dating back to 1950.

3) Given the geographic shifts outlined in both ENSO-related physical and atmospheric tornado outbreak climatologies presented here, a forecast of locations expected to experience more frequent and more impactful tornado activity in a particular season can be inferred based on time of year and ENSO phase. Identification of spatial shifts in tornado activity has been made in previous studies but was limited to only the spring time frame; Muñoz and Enfield (2011) and Lee et al. (2013) studied April and May, and Allen et al. 2015 studied March, April, and May as a whole.

Although the overall result of this research suggests potential for seasonal forecasts of tornado outbreaks, several important caveats need to be considered. First, outlier outbreaks driven by synoptic variability that do not match the overall ENSO/tornado climatology have actually occurred (e.g., 29 March 1998 in southern Minnesota). Additionally, one of the composites of the lifted index indicated widespread instability across much of the continental United States east of the Rocky Mountains during El Niño March, contradicting other atmospheric signals (i.e., southwardly displaced upper-level jet streams and low-level jet development) that would support a southward shift of tornado occurrence. Extensive experimentation in an operational environment is needed before official seasonal tornado forecasts can be disseminated. As more development in this topic area occurs, research efforts should focus on the effective communication of seasonal tornado outbreak risk, with an understanding that tornadoes will occasionally occur outside of climatologically favored areas.

Two further distinct areas of future work have emerged from this research. Although ENSO appears to be a key factor for winter and early spring tornado outbreaks in the United States, the complexities of this research are likely the result of additional areas of localized sea surface temperature anomalies (Banholzer and Donner 2014) that appear to play a role on synoptic-scale atmospheric features associated with outbreaks (e.g., the eastern Pacific Ocean)

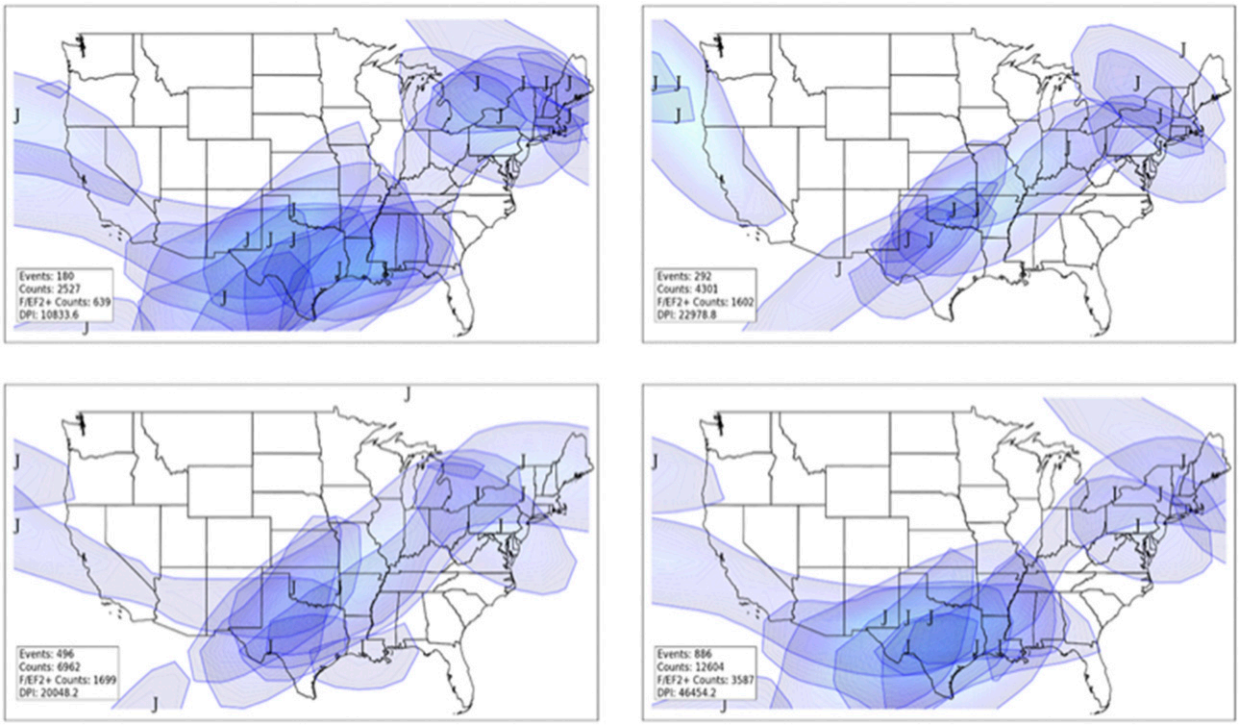

FIG. 17. As in Fig. 10, but for April.

and likely modulate the availability of low-level moisture and potential instability in tornado outbreak development (e.g., the Gulf of Mexico and far western Atlantic Ocean; Elsner and Widen 2014, Lee et al. 2016; Jung and Kirtman 2016; Molina et al. 2016). These factors need to be considered to create a more robust seasonal tornado prediction tool. Additionally, the use of PCA to assess synoptic-scale atmospheric features on a climatological basis has presented interesting possibilities for application of the methodology to 1) develop an environment-based historical tornado record that addresses inaccuracies in historical tornado records in a similar vein as Tippett et al. (2014) and 2) address tornado outbreak risk in future climate scenarios (Brooks 2013; Tippett et al. 2015).

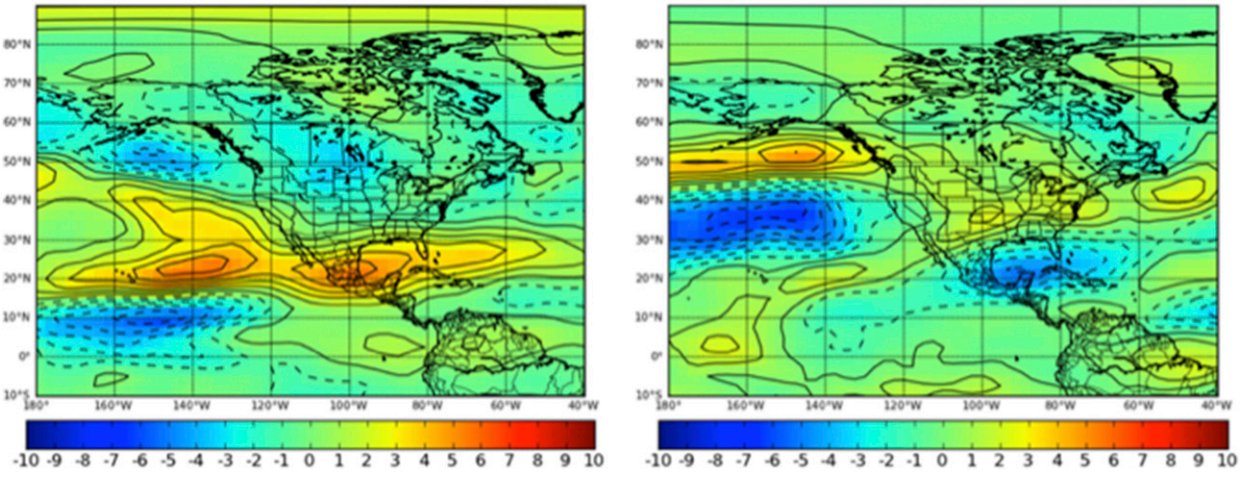

FIG. 18. As in Fig. 8, but for April.

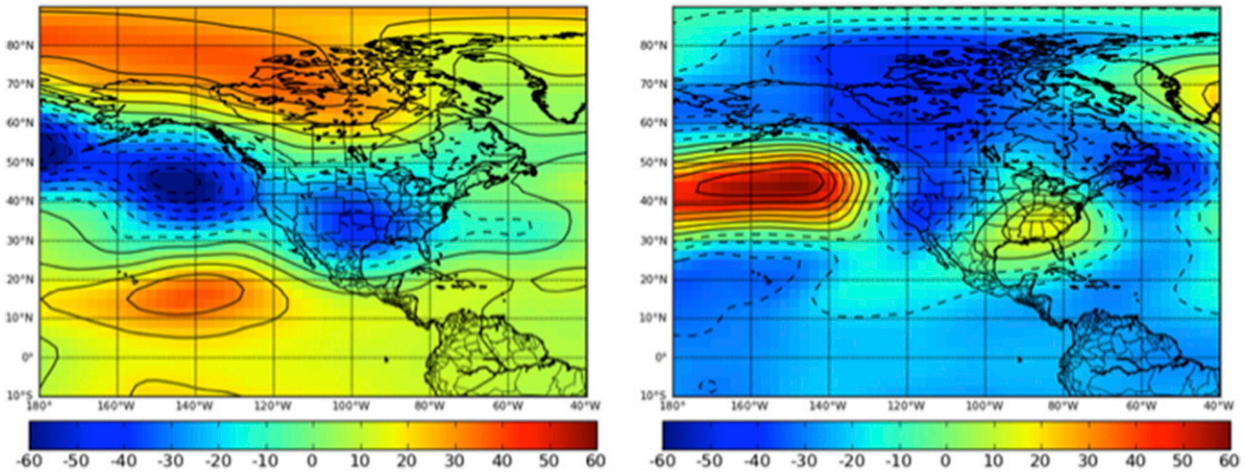

FIG. 19. Monthly anomalies of 500-hPa geopotential height during April (left) El Niño and (right) La Niña conditions.

Acknowledgments. The authors thank the National Weather Service and the Storm Prediction Center for providing support throughout the lead author's graduate studies. The authors also acknowledge the late Dr. Peter J. Lamb as well as Drs. Michael Richman, Lesley Rankin-Hill, Susan Postawko, and Israel Jirak for their multitude of contributions toward the completion of this study. Three anonymous reviewers (especially reviewer 3) provided constructive critiques that improved the overall quality of the paper.

REFERENCES

Allen, J. T., M. K. Tippett, and A. H. Sobel, 2015: Influence of the El Niño/Southern Oscillation on tornado and hail frequency in the United States. *Nat. Geosci.*, **8**, 278–283, doi:10.1038/ngeo2385.

Banholzer, S., and S. Donner, 2014: The influence of different El Niño types on global average temperature. *Geophys. Res. Lett.*, **41**, 2093–2099, doi:10.1002/2014GL059520.

Barrett, B. S., and V. A. Gensini, 2013: Variability of central United States April–May tornado day likelihood by phase of the Madden-Julian Oscillation. *Geophys. Res. Lett.*, **40**, 2790–2795, doi:10.1002/grl.50522.

Bove, M. C., 1998: Impacts of ENSO on United States tornado activity. Preprints, *19th Conf. on Severe Local Storms*, Minneapolis, MN, Amer. Meteor. Soc., 313–316.

Brooks, H. E., 2013: Severe thunderstorms and climate change. *Atmos. Res.*, **123**, 129–138, doi:10.1016/j.atmosres.2012.04.002.

——, C. A. Doswell III, and M. P. Kay, 2003: Climatological estimates of local daily tornado probability for the United States. *Wea. Forecasting*, **18**, 626–640, doi:10.1175/1520-0434(2003)018<0626:CEOLDT>2.0.CO;2.

Cook, A. R., and J. T. Schaefer, 2008: The relation of El Niño–Southern Oscillation (ENSO) to winter tornado outbreaks. *Mon. Wea. Rev.*, **136**, 3121–3137, doi:10.1175/2007MWR2171.1.

Dixon, P. G., A. E. Mercer, J. Choi, and J. S. Allen, 2011: Tornado risk analysis: Is Dixie Alley an extension of Tornado Alley? *Bull. Amer. Meteor. Soc.*, **92**, 433–441, doi:10.1175/2010BAMS3102.1.

Doswell, C. A., III, and D. W. Burgess, 1988: On some issues of the United States tornado climatology. *Mon. Wea. Rev.*, **116**, 495–501, doi:10.1175/1520-0493(1988)116<0495:OSIOUS>2.0.CO;2.

——, R. Edwards, R. L. Thompson, J. A. Hart, and K. C. Crosbie, 2006: A simple and flexible method for ranking severe weather events. *Wea. Forecasting*, **21**, 939–951, doi:10.1175/WAF959.1.

Efron, B., and R. J. Tibshirani, 1993: *An Introduction to the Bootstrap*. Chapman and Hall, 436 pp.

Eichler, T., and R. W. Higgins, 2006: Climatology and ENSO-related variability of North American extratropical cyclone activity. *J. Climate*, **19**, 2076–2093, doi:10.1175/JCLI3725.1.

Elsner, J. B., and H. M. Widen, 2014: Predicting spring tornado activity in the central Great Plains by 1 March. *Mon. Wea. Rev.*, **142**, 259–267, doi:10.1175/MWR-D-13-00014.1.

Fricker, T., and J. B. Elsner, 2015: Kinetic energy of tornadoes in the United States. *PLoS One*, **10**, e0131090, doi:10.1371/journal.pone.0131090.

Galway, J. G., 1956: The lifted index as a predictor of latent instability. *Bull. Amer. Meteor. Soc.*, **43**, 528–529.

——, 1975: Relationship of tornado deaths to severe weather watch areas. *Mon. Wea. Rev.*, **103**, 737–741, doi:10.1175/1520-0493(1975)103<0737:ROTDTS>2.0.CO;2.

——, 1977: Some climatological aspects of tornado outbreaks. *Mon. Wea. Rev.*, **105**, 477–484, doi:10.1175/1520-0493(1977)105<0477:SCAOTO>2.0.CO;2.

Johns, R. H., and C. A. Doswell III, 1992: Severe local storms forecasting. *Wea. Forecasting*, **7**, 588–612, doi:10.1175/1520-0434(1992)007<0588:SLSF>2.0.CO;2.

Jung, E., and B. P. Kirtman, 2016: Can we predict seasonal changes in high impact weather in the United States? *Environ. Res. Lett.*, **11**, 074018, doi:10.1088/1748-9326/11/7/074018.

Kalnay, E., and Coauthors, 1996: The NCEP/NCAR 40-Year Reanalysis Project. *Bull. Amer. Meteor. Soc.*, **77**, 437–471, doi:10.1175/1520-0477(1996)077<0437:TNYRP>2.0.CO;2.

Kellner, O., and D. Niyogi, 2014: Land surface heterogeneity signature in tornado climatology? An illustrative analysis over Indiana, 1950–2012. *Earth Interact.*, **18**, doi:10.1175/2013EI000548.1.

Kelly, D. L., J. T. Schaefer, R. P. McNulty, C. A. Doswell, and R. F. Abbey, 1978: An augmented tornado climatology. *Mon. Wea. Rev.*, **106**, 1172–1183, doi:10.1175/1520-0493(1978)106<1172:AATC>2.0.CO;2.

Knowles, J. B., and R. A. Pielke, 2005: The Southern Oscillation and its effects on tornadic activity in the United States. Colorado State University Atmospheric Sciences Paper 755, 15 pp.

Lee, J. T., and J. G. Galway, 1956: Preliminary report on the relationship between the jet at 200-mb level and tornado occurrence. *Bull. Amer. Meteor. Soc.*, **37**, 327–332.

Lee, S.-K., R. Atlas, D. Enfield, C. Wang, and H. Liu, 2013: Is there an optimal ENSO pattern that enhances large-scale atmospheric processes conducive to tornado outbreaks in the United States? *J. Climate*, **26**, 1626–1642, doi:10.1175/JCLI-D-12-00128.1.

——, A. T. Wittenberg, D. B. Enfield, S. J. Weaver, C. Wang, and R. Atlas, 2016: Springtime U.S. regional tornado outbreaks and their links to ENSO flavors and North Atlantic SST variability. *Environ. Res. Lett.*, **11**, 044008, doi:10.1088/1748-9326/11/4/044008.

Madden, R. A., and P. R. Julian, 1972: Description of global-scale circulation cells in the tropics with a 40–50 day period. *J. Atmos. Sci.*, **29**, 1109–1123, doi:10.1175/1520-0469(1972)029<1109:DOGSCC>2.0.CO;2.

Marzban, C., and J. T. Schaefer, 2001: The correlation between U.S. tornadoes and Pacific sea surface temperatures. *Mon. Wea. Rev.*, **129**, 884–895, doi:10.1175/1520-0493(2001)129<0884:TCBUST>2.0.CO;2.

Miller, R. C., 1972: Notes on analysis and severe storm forecasting procedures of the Air Force Global Weather Central. Tech. Rep. 200 (revised), 190 pp.

Molina, M. J., R. P. Timmer, and J. T. Allen, 2016: Importance of the Gulf of Mexico as a climate driver for U.S. severe thunderstorm activity. *Geophys. Res. Lett.*, **43**, 12 295–12 304, doi:10.1002/2016GL071603.

Montroy, D. L., M. B. Richman, and P. J. Lamb, 1998: Observed nonlinearities of monthly teleconnections between tropical pacific sea surface temperature anomalies and central and eastern North American precipitation. *J. Climate*, **11**, 1812–1835, doi:10.1175/1520-0442(1998)011<1812:ONOMTB>2.0.CO;2.

Muñoz, E., and D. Enfield, 2011: The boreal spring variability of the intra-Americas low-level jet and its relation with precipitation and tornadoes in the eastern United States. *Climate Dyn.*, **36**, 247–259, doi:10.1007/s00382-009-0688-3.

NOAA, 2014: 2011 tornado information. [Available online at http://www.noaanews.noaa.gov/2011_tornado_information.html.]

NOAA/CPC, 2015: El Niño and La Niña-related winter features over North America. [Available online at http://www.cpc.ncep.noaa.gov/products/analysis_monitoring/ensocycle/nawinter.shtml.]

NOAA/NCDC, 2011: Storm events database. [Available online at https://www.ncdc.noaa.gov/stormevents/.]

Pautz, M. E., 1969: Severe local storm occurrences, 1955–1967. Environmental Science Services Administration Tech. Memo. WBTM FCST12, 77 pp.

Rasmusson, E. M., and K. Mo, 1993: Linkages between 200-mb tropical and extratropical circulation anomalies during the 1986–1989 ENSO cycle. *J. Climate*, **6**, 595–616, doi:10.1175/1520-0442(1993)006<0595:LBMTAE>2.0.CO;2.

Richman, M. B., 1986: Rotation of principal components. *J. Climatol.*, **6**, 293–335, doi:10.1002/joc.3370060305.

——, and P. J. Lamb, 1985: Climatic pattern analysis of three- and seven-day summer rainfall in the central United States: Some methodological considerations and a regionalization. *J. Climate Appl. Meteor.*, **24**, 1325–1343, doi:10.1175/1520-0450(1985)024<1325:CPAOTA>2.0.CO;2.

Schaefer, J. T., 1986: Severe thunderstorm forecasting: A historical perspective. *Wea. Forecasting*, **1**, 164–189, doi:10.1175/1520-0434(1986)001<0164:STFAHP>2.0.CO;2.

——, and R. Edwards, 1999: The SPC tornado/severe thunderstorm database. Preprints, *11th Conf. on Applied Climatology*, Dallas, TX, Amer. Meteor. Soc., 215–220.

——, D. L. Kelly, and R. F. Abbey, 1980: *Tornado Track Characteristics and Hazard Probabilities*. Pergamon Press, 650 pp.

Schneider, R. S., J. T. Schaefer, and H. E. Brooks, 2004: Tornado outbreak days: An updated and expanded climatology (1875-2003). *22nd Conf. Severe Local Storms*, St. Louis, MO, Amer. Meteor. Soc., P5.1. [Available online at https://ams.confex.com/ams/11aram22sls/techprogram/paper_82031.htm.]

Sparrow, K. H., and A. E. Mercer, 2016: Predictability of US tornado outbreak seasons using ENSO and northern hemisphere geopotential height variability. *Geosci. Front.*, **7**, 21–31, doi:10.1016/j.gsf.2015.07.007.

Thompson, A., 2016: Experimental forecast projects tornado season. Climate Central, accessed 2 June 2016. [Available online at http://www.climatecentral.org/news/experimental-forecast-projects-tornado-season-18780.]

Thompson, R. L., and M. D. Vescio, 1998. The destruction potential index—A method for comparing tornado days. Preprints, *19th Conf. on Severe Local Storms*, Minneapolis, MN, Amer. Meteor. Soc., 280–282.

Tippett, M. K., A. H. Sobel, and S. J. Camargo, 2012: Association of U.S. tornado occurrence with monthly environmental parameters. *Geophys. Res. Lett.*, **39**, L02801, doi:10.1029/2011GL050368.

——, ——, ——, and J. T. Allen, 2014: An empirical relation between U.S. tornado activity and monthly environmental parameters. *J. Climate*, **27**, 2983–2999, doi:10.1175/JCLI-D-13-00345.1.

——, J. T. Allen, V. A. Gensini, and H. E. Brooks, 2015: Climate and hazardous convective weather. *Curr. Climate Change Rep.*, **1**, 60–73, doi:10.1007/s40641-015-0006-6.

Uccellini, L. W., and D. R. Johnson, 1979: The coupling of upper and lower tropospheric jet streaks and implications for the development of severe convective storms. *Mon. Wea. Rev.*, **107**, 682–703, doi:10.1175/1520-0493(1979)107<0682:TCOUAL>2.0.CO;2.

Verbout, S. M., H. E. Brooks, L. M. Leslie, and D. M. Schultz, 2006: Evolution of the U.S. tornado database: 1954–2003. *Wea. Forecasting*, **21**, 86–93, doi:10.1175/WAF910.1.